A stress-dependent TDP-43 SUMOylation program preserves neuronal function

Authors: Terry R. Suk[1-4], Caroline E. Part[1-4], Trina T. Nguyen[1-4], Jenny L. Zhang[1-4], Meghan M. Heer[1-4], Alejandro Caballero-Gómez[1-4], Veronica S. Grybas[1-4], Paul M. McKeever[5], Benjamin Nguyen[1-4], Steve M. Callaghan[1-4], John M. Woulfe[1,2,6-8], Janice Robertson[5], & Maxime W.C. Rousseaux[1-4]*.

[1]University of Ottawa Brain and Mind Research Institute, ON, Canada

[2]Department of Cellular and Molecular Medicine, University of Ottawa, ON, Canada

[3]Eric Poulin Center for Neuromuscular Diseases, ON, Canada

[4]Ottawa Institute of Systems Biology, ON, Canada

[5]Tanz Centre for Research in Neurodegenerative Diseases, University of Toronto, ON, Canada

[6]The Ottawa Hospital Research Institute, The Ottawa Hospital, ON, Canada

[7]Department of Pathology and Laboratory Medicine, University of Ottawa, ON, Canada

[8]Department of Biochemistry, Microbiology, and Immunology, University of Ottawa, ON, Canada

*Corresponding Author. Email: max.rousseaux@uottawa.ca

Abstract: Amyotrophic Lateral Sclerosis (ALS) and Frontotemporal Dementia (FTD) are overwhelmingly linked to TDP-43 dysfunction. Mutations in TDP-43 are rare, indicating that exogenous factors – such as cellular stressors – converge on TDP-43 to play a key role in disease pathogenesis. Post translational modifications such as SUMOylation play essential roles in response to such exogenous stressors. We therefore set out to understand how SUMOylation may regulate TDP-43 in health and disease. We find that TDP-43 is regulated dynamically via SUMOylation in response to cellular stressors. When this process is blocked *in vivo*, we note age-dependent TDP-43 pathology and sex-specific behavioral deficits linking TDP-43 SUMOylation with aging and disease. Collectively, this work presents TDP-43 SUMOylation as an early physiological response to cellular stress, disruption of which may confer a risk for TDP-43 proteinopathy.

Introduction

TDP-43 is an essential RNA binding protein notorious for its involvement in neurodegenerative diseases. Most notably in Amyotrophic Lateral Sclerosis (ALS) and Frontotemporal Dementia (FTD), TDP-43 is pathologically found mislocalized from the nucleus and aggregated in the cytoplasm of neurons within the central nervous system (CNS) in ~97% and ~45% of disease cases, respectively(*1*, *2*). Furthermore, TDP-43 pathology is increasingly linked to other neurological disorders including Limbic-predominant Age-related TDP-43 Encephalopathy (LATE), Alzheimer's Disease (AD), Chronic Traumatic Encephalopathy (CTE), and Stroke(*3–6*). It is becoming evident that not one, but many mechanisms, including ALS/FTD linked mutations in the gene encoding TDP-43 (*TARDBP*), genetic variants affecting related pathways, and/or environmental factors converge on TDP-43 to cause pathology(*7–12*). Therefore, it is critical to identify molecular pathways that regulate TDP-43. This will yield a better understanding of how their dysfunction contributes to early disease pathogenesis and help uncover novel biomarkers and therapeutic targets directed towards TDP-43.

The formation of cytoplasmic TDP-43 aggregates is increasingly considered a late-stage event in ALS, FTD, and related proteinopathies (herein referred to as ALS/FTD)(*7*). Increasing evidence suggests that the partial mislocalization or complete depletion of TDP-43 from the nucleus to the cytoplasm is an early event in ALS/FTD pathogenesis(*7*, *13–18*). As a result, more efforts have focused on the outcomes of TDP-43 mislocalization as early markers of dysfunction and/or mechanisms driving disease. Indeed, loss of function due to mislocalization of TDP-43 causes aberrant cryptic splicing in genes including *STMN2* and *UNC13A* that can drive the progression of ALS(*14–17*, *19*). Cryptic mis-splicing of *STMN2* was recently found to show better correlation with disease progression compared to classical TDP-43 cytoplasmic aggregates further supporting the need to understand early mechanisms of TDP-43 dysfunction(*20*, *21*).

The earliest events in TDP-43 pathogenesis, upstream of mislocalization, remain convoluted likely due to the coincidence of pathological TDP-43 mislocalization with its normal physiological roles in response to stress(*7*). Thus, mechanisms that may tip this physiological balance towards a pathogenic state likely underlie susceptibility to neurodegeneration. The cellular stress response is a critical pathway tightly linked to ALS/FTD and TDP-43 supported via genetic, experimental, and epidemiological evidence(*22–35*). On one hand, ALS/FTD-linked mutations disrupting various steps of the stress response pathways converge on the dysregulation of TDP-43 resulting in pathology(*22–24*, *29–32*, *35*). On the other hand, exogenous insults such as head injuries, viral infections, and other exposures may confer susceptibility or precipitate ALS/FTD and can serve as pre-clinical models of TDP-43 proteinopathy(*5*, *10*, *11*, *36*). Indeed, prolonged cellular stress due to chronic stress exposure or failures in stress recovery can result in TDP-43 pathology(*27*, *37*). However, much less is known about the roles and direct mechanisms regulating TDP-43 in the cell stress response and how they might be linked to neurodegeneration.

Post translational modifications (PTMs) play key roles in regulating protein function and have been tightly linked to TDP-43 (dys)function and disease. TDP-43 is modified by an array of PTMs including phosphorylation, ubiquitination, acetylation, and polyADP-ribosylation(*38–42*). Abnormal TDP-43 phosphorylation and ubiquitination are pathognomonic of ALS and TDP-43 related FTD(*38*). Recent studies have begun to suggest a role for SUMOylation – the covalent addition of small ubiquitin like modifiers (SUMOs) to lysine residues – in ALS and TDP-43 function, highlighting roles in regulating stress granule disassembly, and TDP-43 splicing and

77 aggregation(*43–47*). SUMOylation is a highly conserved and essential mechanism whereby
78 SUMO proteins are covalently bound to target substrate through a cascade mirroring
79 ubiquitination(*48*, *49*). SUMOylation plays a wide variety of roles in the cell including
80 regulation of cellular stress responses, nucleocytoplasmic transport, and protein solubility(*50*).
81 As these functions strongly overlap with TDP-43 pathobiology and stress response, we posited
82 that SUMOylation has a direct role in regulating TDP-43-mediated stress responses.

83 **TDP-43 is SUMOylated in the nucleus in a context specific manner**

84 Various acute stressors including oxidative (sodium arsenite, $NaAsO_2$), hyperosmotic
85 (D-sorbitol and sodium chloride), and heat shock have been demonstrated to induce TDP-43
86 mislocalization and aggregation *in vitro*, helping to uncover key mechanisms affected in
87 disease(*23*, *51*, *52*). As sodium arsenite is a commonly used stressor to interrogate TDP-43
88 alterations, we examined whether TDP-43 became SUMOylated in response to sodium arsenite
89 treatment. Using an immunoprecipitation assay ("SUMOylation Assay", Fig. 1A) to
90 immunoprecipitate HA-SUMO bound proteins under denaturing conditions to disrupt non-
91 covalent protein interactions, we found that TDP-43 becomes SUMOylated by SUMO2 and can
92 form polySUMO chains specifically in response to sodium arsenite (Fig. 1B). Interestingly we
93 found that sodium arsenite and heat shock stressors, but not hyperosmotic stress, induced
94 TDP-43 SUMOylation suggesting that SUMOylation is a context specific modifier of TDP-43
95 (fig. S1A). We further validated that TDP-43 is SUMOylated by SUMO2 and SUMO3, but not
96 SUMO1, consistent with the roles of SUMO2/3 in response to stress (fig. S1B). Mature
97 (covalently bound) SUMO2 and SUMO3 share nearly 100% amino acid homology making them
98 difficult to differentiate and thus referred together as SUMO2/3. Since SUMO2 is the only
99 essential and most abundantly expressed SUMO paralog in the CNS and sodium arsenite is
100 commonly used to study TDP-43 pathobiology, we focused on TDP-43 SUMOylation by
101 SUMO2 in response to sodium arsenite stress(*53*, *54*).

102 TDP-43 and SUMO2 are widely expressed throughout the nucleus however interactions
103 only occur in response to stress, making co-localization analysis challenging to infer
104 SUMOylation events (fig. S1C). To visualize the interaction between TDP-43 and SUMO2/3 we
105 performed a proximity ligation assay (PLA) in murine primary cortical neurons cultures
106 (Fig. 1C, S1D). We observed that in response to sodium arsenite there is a significant increase in
107 PLA signal between endogenous TDP-43 and SUMO2/3, consistent with an increased TDP-43
108 SUMOylation in response to stress. To connect TDP-43 SUMOylation to disease-like states, we
109 expressed ALS-causing TDP-43^{Q331K} and disrupted the nuclear localization sequence in TDP-43
110 (TDP-43^{NLSmut}) to mislocalize TDP-43 to the cytoplasm and found that in response to sodium
111 arsenite TDP-43^{Q331K} leads to increased TDP-43 SUMOylation, while TDP-43^{NLSmut} blocks
112 SUMOylation indicating that nuclear localization is essential for TDP-43 SUMOylation
113 (Fig. 1D). The latter finding is supported by the nuclear PLA signal indicating TDP-43 and
114 SUMO2/3 interact in the nucleus (Fig. 1C). Together, this demonstrates that TDP-43
115 SUMOylation occurs in the nucleus in a stress-specific manner, suggesting that this modification
116 may be an important early mechanism upstream of proteinopathy.

117 **SUMOylation is an early event in response to stress and helps clear TDP-43 through the**
118 **ubiquitin proteasome system during recovery**

119 Prolonged cellular stress *in vitro* leads to mislocalization of TDP-43 and progressive
120 transition into insoluble aggregates resembling aspects of pathology observed in disease(*18*, *27*,

121 *30*, *32*, *55*). As TDP-43 SUMOylation occurs within the nucleus upstream of nuclear egress, we
122 postulated that SUMOylation would occur upstream of aggregation during prolonged sodium
123 arsenite stress. Indeed, we observed that TDP-43 becomes readily SUMOylated in the first 15-30
124 minutes of the acute stress response upstream of the accumulation of RIPA-insoluble,
125 phosphorylated TDP-43 (fig. S1E). Furthermore, we observed an increase in TDP-43
126 SUMOylation that correlated with the duration of stress. To determine whether SUMOylation
127 occurs in response to relative stress intensity, we performed a dose response assay and found that
128 TDP-43 SUMOylation is proportional to relative stress intensity (fig. S1F). Therefore, the
129 increase in TDP-43 SUMOylation during prolonged stress is likely due to an increased stress
130 burden over time.

131 To determine the fate of SUMOylated TDP-43, we performed a stress-recovery time-
132 course assay where cells were stressed with sodium arsenite for up to 1 hour, then allowed cells
133 to recover. For the first hour during stress recovery, we observed a significant peak in TDP-43
134 SUMOylation indicating that TDP-43 is increasingly SUMOylated and polySUMOylated during
135 stress recovery (Fig. 1E). SUMOylated TDP-43 was not detectable after 3 hours of recovery,
136 suggesting that most of the clearance occurs between hours 2-3 post stress. TDP-43 is known to
137 interact with the SUMO-Targeted Ubiquitin Ligase RNF4 which can polyUbiquitinate
138 SUMOylated proteins to be degraded through the UPS(*56*). To determine whether the UPS
139 functions to clear SUMOylated TDP-43 during stress recovery, we treated cells with the
140 proteasome inhibitor MG132 and monitored TDP-43 SUMOylation during stress and recovery.
141 We observed that SUMOylated TDP-43 was not cleared during post-stress recovery with the
142 addition of MG132 indicating that SUMOylated TDP-43 is marked for degradation by the UPS
143 pathway. Importantly, treatment with MG132 for 1 or 4 hours was not sufficient to induce
144 TDP-43 SUMOylation by itself, consistent with the stress-selective nature of TDP-43
145 SUMOylation. Taken together, TDP-43 SUMOylation occurs early in the stress response which
146 then leads to ubiquitin-targeted clearance during stress recovery demonstrating SUMOylation
147 may be an important mechanism regulating nuclear TDP-43 proteostasis.

148 **Stress-dependent TDP-43 SUMOylation is mediated by select E3 SUMO ligases**

149 E3 SUMO ligases can be essential for SUMOylation of select substrates and enable
150 spatiotemporal regulation. Thus, they may represent critical modulators of TDP-43
151 SUMOylation. We used a dual sgRNA/Cas9 approach to knockout 15 candidate E3 SUMO
152 ligases to screen for loss of TDP-43 SUMOylation (Fig. 1F). As a positive control, knockout of
153 the sole E2 SUMO ligase, UBC9 (encoded by *UBE2I*), led to a near complete loss of TDP-43
154 SUMOylation demonstrating the functionality of the approach. We identified four SUMO E3
155 ligases whose knockout consistently reduced the levels of stress-induced TDP-43 SUMOylation:
156 *EGR2 (KROX20), PIAS1, TRIM28,* and *ZNF451.* EGR2 is linked to the neuromuscular disorder
157 Charcot Marie Tooth Disease and is an immediate early gene rapidly reacting to external cellular
158 stimuli aligning with the early response of TDP-43 SUMOylation upon stress (*57*, *58*). PIAS1 is
159 a canonical, highly conserved E3 SUMO ligase known to play roles in cellular stress
160 responses(*59*). TRIM28 is also a well characterized E3 SUMO ligase which is a predicted
161 interactor of SUMOylated TDP-43 based on the GPS-SUMO2.0 algorithm(*60–62*). ZNF451 is
162 characterized as a stress dependent E3 SUMO ligase specifically promoting polySUMOylation
163 with SUMO2/3. It is sometimes referred to as an "E4 SUMO elongase" which complements our
164 data that TDP-43 is polySUMOylated in response to stress(*63*, *64*). Identification of these
165 putative TDP-43 SUMO ligases supports the robustness of stress-induced TDP-43 SUMOylation

166 and adds layers of nuance into the regulation of TDP-43 with variable routes of modulating
167 TDP-43 functions.

168 **TDP-43 SUMOylation occurs in a conserved region of the C-terminal domain**

169 SUMOylation occurs at lysine (K) residues often residing within a consensus
170 SUMOylation motif, *Ψ*-K-x-D/E (*Ψ*=large hydrophobic residue, x = any amino acid), however it
171 is increasingly recognized that SUMOylation at lysine residues in non-consensus motifs is not
172 uncommon and plays significant roles in regulating protein function(*61*). Using GPS-SUMO
173 (https://sumo.biocuckoo.cn/) to predict likely SUMOylation sites on TDP-43, we identified a
174 consensus SUMOylation motif within the first RNA recognition motif at K136, and a
175 non-consensus SUMOylation motif within the C-terminal domain at K408(*61*, *62*). We
176 expressed mutant forms of TDP-43-GFP blocking the predicted sites by mutating the lysine
177 residue to similarly charged arginine residues: K136R, K408R, and double mutant 2KR. We
178 observed that TDP-43^{K136R} did not block sodium arsenite-induced TDP-43 SUMOylation,
179 however the TDP-43^{K408R} mutant significantly reduced TDP-43 SUMOylation, suggesting K408
180 is the primary site of SUMOylation in response to sodium arsenite stress (Fig. 2A). Importantly,
181 mining two independent unbiased mass spectrometry studies identifying sites of SUMOylation
182 across the proteome also revealed TDP-43 SUMOylation at K408, supporting our findings (*65*,
183 *66*).

184 To address the evolutionary conservation of TDP-43 SUMOylation, we aligned the
185 amino acid sequences of TDP-43 with 300 orthologs from OrthoDB and found that human K408
186 is nearly completely conserved throughout jawed-vertebrates concurrent with the evolution of
187 the C-terminal domain (Fig. 2B, table S1). While this domain harbors the majority of ALS/FTD
188 causing mutations, the residues surrounding K408 display considerably high levels of
189 conservation (~86% pairwise identity) indicating that this motif may play important roles in
190 regulating TDP-43 in vertebrates that may be altered by disease causing mutations (Fig. 2C, 1D,
191 table S1). Consistent with these findings, no missense variants have been identified that disrupt
192 the SUMOylation motif (based on gnomAD v4.0, (*67*)) supporting its robust conservation in the
193 healthy human population. Furthermore, the residues surrounding TDP-43 K408 are enriched for
194 PTM sites, specifically phosphorylation at S403, S404, S409, and S410 which are often
195 phosphorylated in patients with TDP-43 proteinopathy, potentially linking TDP-43
196 SUMOylation with phosphorylation and disease pathogenesis(*38*). To determine whether
197 phosphorylation of TDP-43 at these serine residues interact with SUMOylation at K408, we
198 expressed phospho-dead "4SA" TDP-43 (S403/404/409/410A) and observed that TDP-43^{4SA}
199 exhibits increased SUMOylation following stress (Fig. 2D). Whether phosphorylation functions
200 allosterically to remove SUMO2/3 at K408 or antagonistically to block the SUMOylation
201 recognition site remains unclear. The independent modification by either phosphorylation or
202 SUMOylation may serve as a mechanism to differentially regulate TDP-43 function
203 independently or sequentially in response to stimuli. Thus, while TDP-43 phosphorylation has
204 gained significant attention since its initial discovery(*38*) – in part due to the availability of
205 phospho-specific antibodies – we now show that the C-terminal domain contains a conserved
206 PTM-enriched region where SUMOylation at K408 precedes phosphorylation, revealing
207 additional complexity and nuance to the stimulus-induced regulation of TDP-43.

208 **TDP-43 SUMOylation at K408 supports cellular stress response and recovery**

To understand the cellular and physiological roles of TDP-43 SUMOylation, we generated a knock in mouse model harboring a missense (c.1223 A>G) point mutation in the endogenous mouse *Tardbp* locus resulting in the expression of TDP-43 bearing a p.K408R missense mutation blocking endogenous TDP-43 SUMOylation (Fig. 2E, S2A). For simplicity herein, all genes/proteins will be referred to following their human nomenclature. Although TDP-43 and SUMO2 are independently essential for embryonic development, the "TDP-43^{K408R}" mice are born at normal mendelian ratios indicating that TDP-43 SUMOylation at K408 is not essential for murine embryonic development (fig. S2B)(*53*, *68*).

As TDP-43 SUMOylation responds to, and is cleared during cellular stress and recovery respectively, we posited that SUMOylated TDP-43 plays key roles in these processes. We cultured TDP-43$^{+/+}$ and TDP-43$^{K408R/K408R}$ primary cortical neurons and performed stress and recovery assays to determine how the cell stress response may be affected. Since TDP-43 is critical for the formation of G3BP1+ stress granules, we examined their formation and resolution following stress and recovery(*69*, *70*). We found that stress granules could form in TDP-43$^{K408R/K408R}$ neurons to the same degree as TDP-43$^{+/+}$ neurons, but there was a significant delay in stress granule clearance during recovery (Fig. 2F, S3A, S3B). Despite this deficiency, there was no significant change in neuron viability during recovery (fig. S3E). To our surprise, we also observed a significant increase in RIPA insoluble phosphorylated TDP-43 at 1 hour recovery that was cleared by 3 hours post-stress recovery (Fig. 2G). Based on our previous results that SUMOylation is cleared by the UPS pathway and phosphorylation may function antagonistically with SUMOylation, the increase in phosphorylation during recovery may serve as an alternative method of proteostasis to compensate for loss of SUMOylation. We further observed a significant increase in nuclear TDP-43 foci that were specific to the recovery phase and were exacerbated after 3 hours recovery in the TDP-43$^{K408R/K408R}$ neurons (Fig. 2F, S2C, S2D). Various forms of nuclear TDP-43 bodies are increasingly recognized to be aberrantly regulated in disease and stress states (*21*, *71–73*). Together, this may indicate that TDP-43$^{K408R/K408R}$ neurons appropriately respond to, but not efficiently resolve cellular stress which can render cells vulnerable to further insult.

Blocking TDP-43 SUMOylation *in vivo* leads to sex-specific social and cognitive deficits and TDP-43 proteinopathy reminiscent of FTD

Aging is one of the strongest risk factors for many neurodegenerative diseases including ALS/FTD. The process of aging is known to progressively induce stress on cells, particularly in the nervous system, as cellular functions become impaired or as environmental triggers accumulate over time(*74*). As TDP-43 SUMOylation is involved in supporting the normal cellular stress response and maintaining TDP-43 proteostasis, we hypothesized that disrupting this process leads to age-dependent physiological changes accelerated by impaired stress responses and TDP-43 accumulation.

In young pups, we did not observe any significant differences between TDP-43$^{+/+}$, TDP-43$^{K408R/+}$, or TDP-43$^{K408R/K408R}$ with respect to body weight or motor abilities indicating that blocking TDP-43 SUMOylation does not lead to gross developmental abnormalities (fig. S4). We performed a battery of behavioral tests focusing on motor, social, and cognitive function related to ALS and FTD at three time points (2, 9 and 16 months, fig. S5-S8, table S2). We observed sex-specific cognitive and social effects biased to female animals that generally worsened with aging. Starting around 2 months of age, we observed significant barbering in female mice leading to alopecia in the K408R mutants (Fig. 3A). Consistent with this finding we

254 found that aged female TDP-43$^{K408R/K408R}$ mice were significantly more submissive to their
255 TDP-43$^{+/+}$ counterparts in the tube test (Fig. 3B). Additionally, we observed age dependent
256 changes in behavior, such as significant risk taking and hyperactivity in the open field test at 2
257 months of age (Fig. 3C). This hyperactivity was age-dependent and selectively affected young
258 female mice as they were significantly less active than their TDP-43$^{+/+}$ counterparts at 9 months
259 of age in the open field tests (Fig. 3C). Additionally, these female TDP-43$^{K408R/K408R}$ mice
260 presented with significant impairment in habituation at 9 months in the beam break test
261 (Fig. 3D). By 16 months of age, female TDP-43$^{K408R/K408R}$ mice performed significantly worse
262 than TDP-43$^{+/+}$ mice in the spontaneous Y-maze, inferring age-dependent cognitive decline in
263 the domain of working memory (Fig. 3E). There were no significant cognitive effects in male
264 TDP-43$^{K408R/K408R}$ mice, however impairments were observed on the rotarod test at 9 months of
265 age (fig. S6). This deficiency was not observed at 16 months of age, largely due to all mice
266 performing significantly worse at the rotarod task, limiting interpretation. Taken together, the
267 age-dependent cognitive and social impairment observed in female TDP-43 SUMO-deficient
268 mutants highlight interesting and unexplored aspects of TDP-43 with important implications for
269 understanding sex-specific roles of TDP-43 SUMOylation.

270 Cellular and molecular changes are generally thought to precede behavioral changes in
271 mouse models and human disease. Consistent with the behavioral findings described above, we
272 find that insoluble phosphorylated TDP-43 accumulated in the cortex of female, but not male
273 mice, and mislocalized and phosphorylated TDP-43 could be observed in the lumbar spinal cord
274 of both male and female mice at 9 months of age (Fig. 3F, S9, S10A). At 16 months of age, male
275 TDP-43$^{K408R/K408R}$ mice displayed a significant denervation of neuromuscular junctions in the
276 tibialis anterior and a reduction in ChAT positive neurons in the spinal cord compared to
277 littermate controls (Fig. 3G, fig S10B, S10C). These data support that TDP-43 SUMOylation
278 plays a protective role in mediating TDP-43 proteostasis in the CNS and that its blockade may
279 confer a risk for ALS/FTD-like pathogenesis in an age-dependent, and sex-specific manner
280 providing insights into molecular substrates underlying sexually dimorphic clinical features of
281 ALS and FTD.

282 **Aberrant SUMOylation is a Feature of Human Aging and Disease**

283 Although SUMOylation is well understood to play an essential role in the CNS, its
284 involvement in human aging and neurodegenerative diseases remains largely unknown. To
285 assess how SUMOylation is normally affected in human aging, we processed samples from
286 human temporal lobe tissue ranging between 0.5 and 88 years of age from individuals unaffected
287 by neurological diseases (Fig. 4A, S11A, table S3, n=55). Complementing our findings that
288 SUMOylation serves as a protective feature of aging in our TDP-43^{K408R} model, we observed
289 that global SUMOylation was also positively correlated with age. This supports a link between
290 increased SUMOylation and normal aging in the human brain, possibly as a protective
291 mechanism due to increased proteostasis demand (Fig. 4B).

292 To explore the extent of TDP-43 SUMOylation in human ALS/FTD cases, we performed
293 proximity ligation assays against TDP-43 and SUMO2/3 in prefrontal cortex samples from
294 ALS/FTD cases positive for TDP-43 pathology and age/sex matched unaffected controls
295 (fig. S11B, table S3). Surprisingly, we observed a significant increase in TDP-43 – SUMO2/3
296 interactions in the prefrontal cortex of ALS/FTD patients with TDP-43 pathology (Fig. 4C). This
297 may be a result of increased stress burden throughout the prefrontal cortex in those affected by

298 ALS/FTD with TDP-43 pathology compared to age and sex matched counterparts. Taken
299 together, SUMOylation as a stress responsive modification is positively correlated with aging in
300 the human brain, potentially linked to the increase demand imposed by age-associated stress.
301 Additionally, the SUMOylation response is enhanced in the frontal cortex of those affected by
302 ALS/FTD providing further *in vivo* support for its role in disease.

303 **Discussion**

304 Although ALS and FTD are highly heterogenous diseases, the nearly universal
305 convergence on TDP-43 emphasizes a need to understand early drivers of TDP-43 pathogenesis.
306 Despite this, there remains a gap in knowledge about the mechanisms maintaining proteostatic
307 balance and how their disruption ultimately leads to dysfunction of TDP-43. We found that
308 SUMOylation is a conserved mechanism regulating nuclear TDP-43 function selectively during
309 cellular stress that subsequently promotes UPS-mediated clearance during recovery. Indeed,
310 recent reports have found that other stress related proteins such as G3BP1 are differentially
311 modified by PTMs according to the type of stress that cells are responding to, highlighting
312 unique ways stress-related proteins can execute different functions in a context-specific
313 manner(*75*, *76*). This context-specific regulation provides unique opportunities to understand
314 specific pathways activated in disease that may be therapeutically targeted. Future studies
315 modulating TDP-43 E3 SUMO ligases may help alter the cell stress response, potentially by
316 decreasing aberrant TDP-43 activity or by promoting stress-specific responses to ease the burden
317 in vulnerable cells.

318 SUMOylation of TDP-43 occurs at K408 in a highly conserved region of the C-terminal
319 domain directly adjacent to phosphorylation sites that are characteristically phosphorylated in
320 aggregates in TDP-43 proteinopathies(*38*). We found that phosphorylation and SUMOylation act
321 antagonistically on TDP-43, indicating potential distinct mechanisms of regulation. As
322 SUMOylated TDP-43 is cleared by the UPS-pathway during stress recovery we hypothesized
323 that blocking TDP-43 SUMOylation with K408R mutation would result in its accumulation
324 during stress recovery. Interestingly, we observed a significant increase in insoluble
325 phosphorylated TDP-43 in TDP-43$^{K408R/K408R}$ cortical neurons and a delay in stress granule
326 disassembly during stress recovery indicating TDP-43 accumulation. However, this was resolved
327 3 hours post-stress indicating that the neurons could compensate to clear the aberrantly
328 accumulated TDP-43 within this acute stress paradigm. Future studies exploring repeated and/or
329 divergent stressors will be crucial in determining the degree to which TDP-43 SUMOylation
330 safeguards from cellular demise.

331 Previous reports have emphasized the status of altered proteostasis as a hallmark of aging
332 in the CNS, culminating in impaired removal of damaged proteins with age(*74*). In
333 TDP-43$^{K408R/K408R}$ mice, TDP-43 was found to accumulate in the CNS in an age-dependent
334 manner. TDP-43 accumulation within the CNS progresses with age, inferring an age-dependent
335 requirement for SUMOylation to maintain proteostasis. Indeed, in human temporal lobe samples,
336 we similarly observed a positive correlation between global SUMOylation and age supporting
337 SUMOylation as a potential protective mechanism during aging in the CNS. However, directly
338 monitoring SUMOylation events remains challenging due to the dynamic nature of the
339 modification and lack of specific tools to study its interaction. We employed a PLA approach to
340 assess the interaction between TDP-43 and SUMO in ALS/FTD patients and found significantly
341 increased interactions in the prefrontal cortex relative to age/sex matched unaffected controls.
342 Recent studies have used RNA aptamers to reveal nuclear changes in TDP-43 in spinal and

cortical neurons of ALS patients prior to traditional cytoplasmic pathology in vulnerable cells(*21*). Further development of these technologies with respect to TDP-43 SUMOylation may help advance biomarker development that can provide information about TDP-43 stress-response and pathogenesis in ALS/FTD patients.

The emergence of predominantly cognitive FTD-like phenotypes in the TDP-43^{K408R} mice is not unusual compared to other TDP-43 knock in models such as TDP-43^{Q331K} and TDP-43^{K145R} mice which present with features of cognitive dysfunction but lacking the entire constellation of ALS/FTD-like phenotypes(*41*, *77*). Though we initially hypothesized that aging may be a sufficient stressor to interrogate TDP-43 SUMOylation in mice, the various stressors that individuals with ALS/FTD were previously exposed to during their lifetime (i.e. the "exposome") are not experienced by mice in vivaria on a short timescale(*69*). The TDP-43^{K408R} model will therefore facilitate the exploration of how the exposome synergizes with TDP-43 to better understand how ALS/FTD relevant stressors (e.g. *C9ORF72* expansions, viral infections, and traumatic brain injury) converge on TDP-43 and uniquely drive neurodegeneration.

References

1. O. Hardiman, A. Al-Chalabi, A. Chio, E. M. Corr, G. Logroscino, W. Robberecht, P. J. Shaw, Z. Simmons, L. H. Van Den Berg, Amyotrophic lateral sclerosis. *Nature Reviews Disease Primers 2017 3:1* **3**, 1–19 (2017).
2. M. Grossman, W. W. Seeley, A. L. Boxer, A. E. Hillis, D. S. Knopman, P. A. Ljubenov, B. Miller, O. Piguet, R. Rademakers, J. L. Whitwell, H. Zetterberg, J. C. van Swieten, Frontotemporal lobar degeneration. *Nature Reviews Disease Primers 2023 9:1* **9**, 1–19 (2023).
3. P. T. Nelson, D. W. Dickson, J. Q. Trojanowski, C. R. Jack, P. A. Boyle, K. Arfanakis, R. Rademakers, I. Alafuzoff, J. Attems, C. Brayne, I. T. S. Coyle-Gilchrist, H. C. Chui, D. W. Fardo, M. E. Flanagan, G. Halliday, S. R. K. Hokkanen, S. Hunter, G. A. Jicha, Y. Katsumata, C. H. Kawas, C. D. Keene, G. G. Kovacs, W. A. Kukull, A. I. Levey, N. Makkinejad, T. J. Montine, S. Murayama, M. E. Murray, S. Nag, R. A. Rissman, W. W. Seeley, R. A. Sperling, C. L. White Iii, L. Yu, J. A. Schneider, Limbic-predominant age-related TDP-43 encephalopathy (LATE): consensus working group report. doi: 10.1093/brain/awz099.
4. A. Meneses, S. Koga, J. O'Leary, D. W. Dickson, G. Bu, N. Zhao, TDP-43 Pathology in Alzheimer's Disease. *Molecular Neurodegeneration 2021 16:1* **16**, 1–15 (2021).
5. R. Nicks, N. F. Clement, V. E. Alvarez, Y. Tripodis, Z. H. Baucom, B. R. Huber, J. Mez, M. L. Alosco, N. Aytan, J. D. Cherry, K. A. Cormier, C. Kubilius, R. Mathias, S. E. Svirsky, M. J. Pothast, A. M. Hildebrandt, J. Chung, X. Han, J. F. Crary, A. C. McKee, M. P. Frosch, T. D. Stein, Repetitive head impacts and chronic traumatic encephalopathy are associated with TDP-43 inclusions and hippocampal sclerosis. *Acta Neuropathol* **145**, 395–408 (2023).
6. S. S. Thammisetty, J. Pedragosa, Y. C. Weng, F. Calon, A. Planas, J. Kriz, Age-related deregulation of TDP-43 after stroke enhances NF-κB-mediated inflammation and neuronal damage. *J Neuroinflammation* **15**, 1–15 (2018).
7. T. R. Suk, M. W. C. Rousseaux, The role of TDP-43 mislocalization in amyotrophic lateral sclerosis. *Mol Neurodegener* **15**, 45 (2020).

8. J. Chew, T. F. Gendron, M. Prudencio, H. Sasaguri, Y. J. Zhang, M. Castanedes-Casey, C. W. Lee, K. Jansen-West, A. Kurti, M. E. Murray, K. F. Bieniek, P. O. Bauer, E. C. Whitelaw, L. Rousseau, J. N. Stankowski, C. Stetler, L. M. Daughrity, E. A. Perkerson, P. Desaro, A. Johnston, K. Overstreet, D. Edbauer, R. Rademakers, K. B. Boylan, D. W. Dickson, J. D. Fryer, L. Petrucelli, C9ORF72 repeat expansions in mice cause TDP-43 pathology, neuronal loss, and behavioral deficits. *Science (1979)* **348**, 1151–1154 (2015).
9. W. Shao, T. W. Todd, Y. Wu, C. Y. Jones, J. Tong, K. Jansen-West, L. M. Daughrity, J. Park, Y. Koike, A. Kurti, M. Yue, M. Castanedes-Casey, G. del Rosso, J. A. Dunmore, D. Z. Alepuz, B. Oskarsson, D. W. Dickson, C. N. Cook, M. Prudencio, T. F. Gendron, J. D. Fryer, Y. J. Zhang, L. Petrucelli, Two FTD-ALS genes converge on the endosomal pathway to induce TDP-43 pathology and degeneration. *Science (1979)* **378**, 94–99 (2022).
10. G. Fung, J. Shi, H. Deng, J. Hou, C. Wang, A. Hong, J. Zhang, W. Jia, H. Luo, Cytoplasmic translocation, aggregation, and cleavage of TDP-43 by enteroviral proteases modulate viral pathogenesis. *Cell Death & Differentiation 2015 22:12* **22**, 2087–2097 (2015).
11. P. E. A. Ash, E. A. Stanford, A. Al Abdulatif, A. Ramirez-Cardenas, H. I. Ballance, S. Boudeau, A. Jeh, J. M. Murithi, Y. Tripodis, G. J. Murphy, D. H. Sherr, B. Wolozin, Dioxins and related environmental contaminants increase TDP-43 levels. *Mol Neurodegener* **12**, 1–14 (2017).
12. J. Sreedharan, I. P. Blair, V. B. Tripathi, X. Hu, C. Vance, B. Rogelj, S. Ackerley, J. C. Durnall, K. L. Williams, E. Buratti, F. Baralle, J. De Belleroche, J. D. Mitchell, P. N. Leigh, A. Al-Chalabi, C. C. Miller, G. Nicholson, C. E. Shaw, TDP-43 mutations in familial and sporadic amyotrophic lateral sclerosis. *Science (1979)* **319**, 1668–1672 (2008).
13. A. N. Coyne, V. Baskerville, B. L. Zaepfel, D. W. Dickson, F. Rigo, F. Bennett, C. Patrick Lusk, J. D. Rothstein, Nuclear accumulation of CHMP7 initiates nuclear pore complex injury and subsequent TDP-43 dysfunction in sporadic and familial ALS. *Sci Transl Med* **13**, 1923 (2021).
14. X. R. Ma, M. Prudencio, Y. Koike, S. C. Vatsavayai, G. Kim, F. Harbinski, A. Briner, C. M. Rodriguez, C. Guo, T. Akiyama, H. B. Schmidt, B. B. Cummings, D. W. Wyatt, K. Kurylo, G. Miller, S. Mekhoubad, N. Sallee, G. Mekonnen, L. Ganser, J. D. Rubien, K. Jansen-West, C. N. Cook, S. Pickles, B. Oskarsson, N. R. Graff-Radford, B. F. Boeve, D. S. Knopman, R. C. Petersen, D. W. Dickson, J. Shorter, S. Myong, E. M. Green, W. W. Seeley, L. Petrucelli, A. D. Gitler, TDP-43 represses cryptic exon inclusion in the FTD–ALS gene UNC13A. *Nature 2022 603:7899* **603**, 124–130 (2022).
15. A. L. Brown, O. G. Wilkins, M. J. Keuss, S. E. Hill, M. Zanovello, W. C. Lee, A. Bampton, F. C. Y. Lee, L. Masino, Y. A. Qi, S. Bryce-Smith, A. Gatt, M. Hallegger, D. Fagegaltier, H. Phatnani, H. Phatnani, J. Kwan, D. Sareen, J. R. Broach, Z. Simmons, X. Arcila-Londono, E. B. Lee, V. M. Van Deerlin, N. A. Shneider, E. Fraenkel, L. W. Ostrow, F. Baas, N. Zaitlen, J. D. Berry, A. Malaspina, P. Fratta, G. A. Cox, L. M. Thompson, S. Finkbeiner, E. Dardiotis, T. M. Miller, S. Chandran, S. Pal, E. Hornstein, D. J. MacGowan, T. Heiman-Patterson, M. G. Hammell, N. A. Patsopoulos, O. Butovsky, J. Dubnau, A. Nath, R.

Bowser, M. Harms, E. Aronica, M. Poss, J. Phillips-Cremins, J. Crary, N. Atassi, D. J. Lange, D. J. Adams, L. Stefanis, M. Gotkine, R. H. Baloh, S. Babu, T. Raj, S. Paganoni, O. Shalem, C. Smith, B. Zhang, B. Harris, I. Broce, V. Drory, J. Ravits, C. McMillan, V. Menon, L. Wu, S. Altschuler, Y. Lerner, R. Sattler, K. Van Keuren-Jensen, O. Rozenblatt-Rosen, K. Lindblad-Toh, K. Nicholson, P. Gregersen, J. H. Lee, S. Kokos, S. Muljo, J. Newcombe, E. K. Gustavsson, S. Seddighi, J. F. Reyes, S. L. Coon, D. Ramos, G. Schiavo, E. M. C. Fisher, T. Raj, M. Secrier, T. Lashley, J. Ule, E. Buratti, J. Humphrey, M. E. Ward, P. Fratta, TDP-43 loss and ALS-risk SNPs drive mis-splicing and depletion of UNC13A. *Nature 2022 603:7899* **603**, 131–137 (2022).

16. Z. Melamed, J. López-Erauskin, M. W. Baughn, O. Zhang, K. Drenner, Y. Sun, F. Freyermuth, M. A. McMahon, M. S. Beccari, J. W. Artates, T. Ohkubo, M. Rodriguez, N. Lin, D. Wu, C. F. Bennett, F. Rigo, S. Da Cruz, J. Ravits, C. Lagier-Tourenne, D. W. Cleveland, Premature polyadenylation-mediated loss of stathmin-2 is a hallmark of TDP-43-dependent neurodegeneration. *Nat Neurosci*, 1 (2019).

17. J. R. Klim, L. A. Williams, F. Limone, I. Guerra San Juan, B. N. Davis-Dusenbery, D. A. Mordes, A. Burberry, M. J. Steinbaugh, K. K. Gamage, R. Kirchner, R. Moccia, S. H. Cassel, K. Chen, B. J. Wainger, C. J. Woolf, K. Eggan, ALS-implicated protein TDP-43 sustains levels of STMN2, a mediator of motor neuron growth and repair. *Nat Neurosci* **22**, 167–179 (2019).

18. F. Gasset-Rosa, S. Lu, H. Yu, C. Chen, Z. Melamed, L. Guo, J. Shorter, S. Da Cruz, D. W. Cleveland, Cytoplasmic TDP-43 De-mixing Independent of Stress Granules Drives Inhibition of Nuclear Import, Loss of Nuclear TDP-43, and Cell Death. *Neuron* **102**, 339-357.e7 (2019).

19. M. W. Baughn, Z. Melamed, J. López-Erauskin, M. S. Beccari, K. Ling, A. Zuberi, M. Presa, E. Gonzalo-Gil, R. Maimon, S. Vazquez-Sanchez, S. Chaturvedi, M. Bravo-Hernández, V. Taupin, S. Moore, J. W. Artates, E. Acks, I. Sandra Ndayambaje, A. R. Agra de Almeida Quadros, P. Jafar-Nejad, F. Rigo, C. Frank Bennett, C. Lutz, C. Lagier-Tourenne, D. W. Cleveland, Mechanism of STMN2 cryptic splice-polyadenylation and its correction for TDP-43 proteinopathies. *Science (1979)* **379**, 1140–1149 (2023).

20. A. R. Agra Almeida Quadros, Z. Li, X. Wang, I. S. Ndayambaje, S. Aryal, N. Ramesh, M. Nolan, R. Jayakumar, Y. Han, H. Stillman, C. Aguilar, H. J. Wheeler, T. Connors, J. Lopez-Erauskin, M. W. Baughn, Z. Melamed, M. S. Beccari, L. Olmedo Martínez, M. Canori, C. Z. Lee, L. Moran, I. Draper, A. S. Kopin, D. H. Oakley, D. W. Dickson, D. W. Cleveland, B. T. Hyman, S. Das, N. Ertekin-Taner, C. Lagier-Tourenne, Cryptic splicing of stathmin-2 and UNC13A mRNAs is a pathological hallmark of TDP-43-associated Alzheimer's disease. *Acta Neuropathologica 2024 147:1* **147**, 1–18 (2024).

21. H. Spence, F. M. Waldron, R. S. Saleeb, A. L. Brown, O. M. Rifai, M. Gilodi, F. Read, K. Roberts, G. Milne, D. Wilkinson, J. O'Shaughnessy, A. Pastore, P. Fratta, N. Shneider, G. G. Tartaglia, E. Zacco, M. H. Horrocks, J. M. Gregory, RNA aptamer reveals nuclear TDP-43 pathology is an early aggregation event that coincides with STMN-2 cryptic splicing and precedes clinical manifestation in ALS. *Acta Neuropathol* **147**, 1–15 (2024).

22. I. R. Mackenzie, A. M. Nicholson, M. Sarkar, J. Messing, M. D. Purice, C. Pottier, K. Annu, M. Baker, R. B. Perkerson, A. Kurti, B. J. Matchett, T. Mittag, J. Temirov, G. Y. R. Hsiung, C. Krieger, M. E. Murray, M. Kato, J. D. Fryer, L. Petrucelli, L. Zinman, S. Weintraub, M. Mesulam, J. Keith, S. A. Zivkovic, V. Hirsch-Reinshagen, R. P. Roos, S. Züchner, N. R. Graff-Radford, R. C. Petersen, R. J. Caselli, Z. K. Wszolek, E. Finger, C. Lippa, D. Lacomis, H. Stewart, D. W. Dickson, H. J. Kim, E. Rogaeva, E. Bigio, K. B. Boylan, J. P. Taylor, R. Rademakers, TIA1 Mutations in Amyotrophic Lateral Sclerosis and Frontotemporal Dementia Promote Phase Separation and Alter Stress Granule Dynamics. *Neuron* **95**, 808-816.e9 (2017).
23. A. K. Walker, K. Y. Soo, V. Sundaramoorthy, S. Parakh, Y. Ma, M. A. Farg, R. H. Wallace, P. J. Crouch, B. J. Turner, M. K. Horne, J. D. Atkin, ALS-associated TDP-43 induces endoplasmic reticulum stress, which drives cytoplasmic TDP-43 accumulation and stress granule formation. *PLoS One* **8**, e81170 (2013).
24. O. H. Tam, N. V. Rozhkov, R. Shaw, D. Kim, I. Hubbard, S. Fennessey, N. Propp, H. Phatnani, J. Kwan, D. Sareen, J. R. Broach, Z. Simmons, X. Arcila-Londono, E. B. Lee, V. M. Van Deerlin, N. A. Shneider, E. Fraenkel, L. W. Ostrow, F. Baas, N. Zaitlen, J. D. Berry, A. Malaspina, P. Fratta, G. A. Cox, L. M. Thompson, S. Finkbeiner, E. Dardiotis, T. M. Miller, S. Chandran, S. Pal, E. Hornstein, D. J. MacGowan, T. Heiman-Patterson, M. G. Hammell, N. A. Patsopoulos, O. Butovsky, J. Dubnau, A. Nath, R. Bowser, M. Harms, E. Aronica, M. Poss, J. Phillips-Cremins, J. Crary, N. Atassi, D. J. Lange, D. J. Adams, L. Stefanis, M. Gotkine, R. Baloh, S. Babu, T. Raj, S. Paganoni, O. Shalem, C. Smith, B. Zhang, B. T. Harris, D. Fagegaltier, J. Ravits, J. Dubnau, M. Gale Hammell, Postmortem Cortex Samples Identify Distinct Molecular Subtypes of ALS: Retrotransposon Activation, Oxidative Stress, and Activated Glia. *Cell Rep* **29**, 1164-1177.e5 (2019).
25. B. Wolozin, P. Ivanov, Stress granules and neurodegeneration. Nature Publishing Group [Preprint] (2019). https://doi.org/10.1038/s41583-019-0222-5.
26. M. T. Lin, M. F. Beal, Mitochondrial dysfunction and oxidative stress in neurodegenerative diseases. Nature Publishing Group [Preprint] (2006). https://doi.org/10.1038/nature05292.
27. A. Ratti, V. Gumina, P. Lenzi, P. Bossolasco, F. Fulceri, C. Volpe, D. Bardelli, F. Pregnolato, A. M. Maraschi, F. Fornai, V. Silani, C. Colombrita, Chronic stress induces formation of stress granules and pathological TDP-43 aggregates in human ALS fibroblasts and iPSC-motoneurons. *Neurobiol Dis* **145**, 105051 (2020).
28. E. D'Amico, P. Factor-Litvak, R. M. Santella, H. Mitsumoto, Clinical perspective on oxidative stress in sporadic amyotrophic lateral sclerosis. NIH Public Access [Preprint] (2013). https://doi.org/10.1016/j.freeradbiomed.2013.06.029.
29. C. Colombrita, E. Zennaro, C. Fallini, M. Weber, A. Sommacal, E. Buratti, V. Silani, A. Ratti, TDP-43 is recruited to stress granules in conditions of oxidative insult. *J Neurochem* **111**, 1051–1061 (2009).
30. X. Zuo, J. Zhou, Y. Li, K. Wu, Z. Chen, Z. Luo, X. Zhang, Y. Liang, M. A. Esteban, Y. Zhou, X. D. Fu, TDP-43 aggregation induced by oxidative stress causes global mitochondrial imbalance in ALS. *Nature Structural & Molecular Biology 2021 28:2* **28**, 132–142 (2021).

31. T. Ueda, T. Takeuchi, N. Fujikake, M. Suzuki, E. N. Minakawa, M. Ueyama, Y. Fujino, N. Kimura, S. Nagano, A. Yokoseki, O. Onodera, H. Mochizuki, T. Mizuno, K. Wada, Y. Nagai, Dysregulation of stress granule dynamics by DCTN1 deficiency exacerbates TDP-43 pathology in Drosophila models of ALS/FTD. *Acta Neuropathol Commun* **12**, 1–15 (2024).
32. Y. Iguchi, M. Katsuno, S. Takagi, S. Ishigaki, J. ichi Niwa, M. Hasegawa, F. Tanaka, G. Sobue, Oxidative stress induced by glutathione depletion reproduces pathological modifications of TDP-43 linked to TDP-43 proteinopathies. *Neurobiol Dis* **45**, 862–870 (2012).
33. L. Liu-Yesucevitz, A. Bilgutay, Y. J. Zhang, T. Vanderwyde, A. Citro, T. Mehta, N. Zaarur, A. McKee, R. Bowser, M. Sherman, L. Petrucelli, B. Wolozin, Tar DNA binding protein-43 (TDP-43) associates with stress granules: Analysis of cultured cells and pathological brain tissue. *PLoS One* **5**, e13250 (2010).
34. K. K. McDonald, A. Aulas, L. Destroismaisons, S. Pickles, E. Beleac, W. Camu, G. A. Rouleau, C. Vande Velde, TAR DNA-binding protein 43 (TDP-43) regulates stress granule dynamics via differential regulation of G3BP and TIA-1. *Hum Mol Genet* **20**, 1400–1410 (2011).
35. W. Luan, A. L. Wright, H. Brown-Wright, S. Le, R. San Gil, L. Madrid San Martin, K. Ling, P. Jafar-Nejad, F. Rigo, A. K. Walker, Early activation of cellular stress and death pathways caused by cytoplasmic TDP-43 in the rNLS8 mouse model of ALS and FTD. *Molecular Psychiatry 2023 28:6* **28**, 2445–2461 (2023).
36. A. Dubinski, M. Gagne, S. Peyrard, D. Gordon, K. Talbot, C. Vande Velde, Stress granule assembly in vivo is deficient in the CNS of mutant TDP-43 ALS mice. *Hum Mol Genet* **32**, 319–332 (2023).
37. P. Zhang, B. Fan, P. Yang, J. Temirov, J. Messing, H. J. Kim, J. P. Taylor, Chronic optogenetic induction of stress granules is cytotoxic and reveals the evolution of ALS-FTD pathology. *Elife* **8** (2019).
38. M. Neumann, L. K. Kwong, E. B. Lee, E. Kremmer, A. Flatley, Y. Xu, M. S. Forman, D. Troost, H. A. Kretzschmar, J. Q. Trojanowski, V. M. Y. Lee, Phosphorylation of S409/410 of TDP-43 is a consistent feature in all sporadic and familial forms of TDP-43 proteinopathies. *Acta Neuropathol* **117**, 137–149 (2009).
39. M. Neumann, D. M. Sampathu, L. K. Kwong, A. C. Truax, M. C. Micsenyi, T. T. Chou, J. Bruce, T. Schuck, M. Grossman, C. M. Clark, L. F. McCluskey, B. L. Miller, E. Masliah, I. R. Mackenzie, H. Feldman, W. Feiden, H. A. Kretzschmar, J. Q. Trojanowski, V. M.-Y. Lee, Ubiquitinated TDP-43 in Frontotemporal Lobar Degeneration and Amyotrophic Lateral Sclerosis. *Science (1979)* **314**, 130–133 (2006).
40. T. Arai, M. Hasegawa, H. Akiyama, K. Ikeda, T. Nonaka, H. Mori, D. Mann, K. Tsuchiya, M. Yoshida, Y. Hashizume, T. Oda, TDP-43 is a component of ubiquitin-positive tau-negative inclusions in frontotemporal lobar degeneration and amyotrophic lateral sclerosis. *Biochem Biophys Res Commun* **351**, 602–611 (2006).
41. J. Necarsulmer, J. Simon, B. Evangelista, Y. Chen, X. Tian, S. Nafees, A. M. Gonzalez, H. Jiang, P. Wang, D. Ajit, V. Nikolova, K. Harper, J. Ezzell, F.-C. Lin, A. Beltran, S. Moy, T. Cohen, RNA-binding deficient TDP-43 drives cognitive decline in a mouse model of TDP-43 proteinopathy. *Elife* **12** (2023).

42. L. McGurk, E. Gomes, L. Guo, J. Mojsilovic-Petrovic, V. Tran, R. G. Kalb, J. Shorter, N. M. Bonini, Poly(ADP-Ribose) Prevents Pathological Phase Separation of TDP-43 by Promoting Liquid Demixing and Stress Granule Localization. *Mol Cell* **71**, 703-717.e9 (2018).
43. H. Marmor-Kollet, A. Siany, N. Kedersha, N. Knafo, N. Rivkin, Y. M. Danino, T. G. Moens, T. Olender, D. Sheban, N. Cohen, T. Dadosh, Y. Addadi, R. Ravid, C. Eitan, B. Toth Cohen, S. Hofmann, C. L. Riggs, V. M. Advani, A. Higginbottom, J. Cooper-Knock, J. H. Hanna, Y. Merbl, L. Van Den Bosch, P. Anderson, P. Ivanov, T. Geiger, E. Hornstein, Spatiotemporal Proteomic Analysis of Stress Granule Disassembly Using APEX Reveals Regulation by SUMOylation and Links to ALS Pathogenesis. *Mol Cell* **80**, 876-891.e6 (2020).
44. A. Osmanovic, A. Förster, M. Widjaja, B. Auber, · Anibh, M. Das, A. Christians, · Frank Brand, S. Petri, R. G. Weber, A SUMO4 initiator codon variant in amyotrophic lateral sclerosis reduces SUMO4 expression and alters stress granule dynamics. *Journal of Neurology 2022* **1**, 1–9 (2022).
45. A. M. Maraschi, V. Gumina, J. Dragotto, C. Colombrita, M. Mompeán, E. Buratti, V. Silani, M. Feligioni, A. Ratti, SUMOylation Regulates TDP-43 Splicing Activity and Nucleocytoplasmic Distribution. *Mol Neurobiol* **58**, 5682–5702 (2021).
46. C. Maurel, A. A. Chami, R. A. Thépault, S. Marouillat, H. Blasco, P. Corcia, C. R. Andres, P. Vourc'h, A role for SUMOylation in the Formation and Cellular Localization of TDP-43 Aggregates in Amyotrophic Lateral Sclerosis. *Mol Neurobiol* **57**, 1361–1373 (2020).
47. N. T. Seyfried, Y. M. Gozal, E. B. Dammer, Q. Xia, D. M. Duong, D. Cheng, J. J. Lah, A. I. Levey, J. Peng, Multiplex SILAC analysis of a cellular TDP-43 proteinopathy model reveals protein inclusions associated with SUMOylation and diverse polyubiquitin chains. *Molecular and Cellular Proteomics* **9**, 705–718 (2010).
48. J. M. Henley, T. J. Craig, K. A. Wilkinson, Neuronal SUMOylation: mechanisms, physiology, and roles in neuronal dysfunction. American Physiological Society Bethesda, MD [Preprint] (2014). https://doi.org/10.1152/physrev.00008.2014.
49. K. A. Wilkinson, J. M. Henley, Mechanisms, regulation and consequences of protein SUMOylation. *Biochemical Journal* **428**, 133–145 (2010).
50. J. M. Enserink, Sumo and the cellular stress response. BioMed Central Ltd. [Preprint] (2015). https://doi.org/10.1186/s13008-015-0010-1.
51. C. M. Dewey, B. Cenik, C. F. Sephton, D. R. Dries, P. Mayer, S. K. Good, B. A. Johnson, J. Herz, G. Yu, TDP-43 Is Directed to Stress Granules by Sorbitol, a Novel Physiological Osmotic and Oxidative Stressor. *Mol Cell Biol* **31**, 1098–1108 (2011).
52. H. Y. Chang, S. C. Hou, T. Der Way, C. H. Wong, I. F. Wang, Heat-shock protein dysregulation is associated with functional and pathological TDP-43 aggregation. *Nat Commun* **4**, 1–11 (2013).
53. L. Wang, C. Wansleeben, S. Zhao, P. Miao, W. Paschen, W. Yang, SUMO 2 is essential while SUMO 3 is dispensable for mouse embryonic development . *EMBO Rep* **15**, 878–885 (2014).
54. T. R. Suk, T. T. Nguyen, Z. A. Fisk, M. Mitkovski, H. M. Geertsma, J. L. A. Parmasad, M. M. Heer, S. M. Callaghan, F. Benseler, N. Brose, M. Tirard, M. W.

616 C. Rousseaux, Characterizing the differential distribution and targets of Sumo1 and
617 Sumo2 in the mouse brain. *iScience* **26**, 106350 (2023).
618 55. J. R. Mann, A. M. Gleixner, J. C. Mauna, E. Gomes, M. R. DeChellis-Marks, P. G.
619 Needham, K. E. Copley, B. Hurtle, B. Portz, N. J. Pyles, L. Guo, C. B. Calder, Z. P.
620 Wills, U. B. Pandey, J. K. Kofler, J. L. Brodsky, A. Thathiah, J. Shorter, C. J.
621 Donnelly, RNA Binding Antagonizes Neurotoxic Phase Transitions of TDP-43.
622 *Neuron* **102**, 321-338.e8 (2019).
623 56. J. Keiten-Schmitz, K. Wagner, T. Piller, M. Kaulich, S. Alberti, S. Müller, The
624 Nuclear SUMO-Targeted Ubiquitin Quality Control Network Regulates the
625 Dynamics of Cytoplasmic Stress Granules. *Mol Cell* **79**, 54-67.e7 (2020).
626 57. L. E. Warner, P. Mancias, I. J. Butler, C. M. McDonald, L. Keppen, K. G. Koob, J.
627 R. Lupski, Mutations in the early growth response 2 (EGR2) gene are associated
628 with hereditary myelinopathies. *Nature Genetics 1998 18:4* **18**, 382–384 (1998).
629 58. P. Garcáa-Gutiérrez, F. Juárez-Vicente, F. Gallardo-Chamizo, P. Charnay, M.
630 García-Domínguez, The transcription factor Krox20 is an E3 ligase that sumoylates
631 its Nab coregulators. *EMBO Rep* **12**, 1018–1023 (2011).
632 59. T. Nishida, H. Yasuda, PIAS1 and PIASxα Function as SUMO-E3 Ligases toward
633 Androgen Receptor and Repress Androgen Receptor-dependent Transcription.
634 *Journal of Biological Chemistry* **277**, 41311–41317 (2002).
635 60. Q. Liang, H. Deng, X. Li, X. Wu, Q. Tang, T.-H. Chang, H. Peng, F. J. Rauscher,
636 K. Ozato, F. Zhu, Tripartite Motif-Containing Protein 28 Is a Small Ubiquitin-
637 Related Modifier E3 Ligase and Negative Regulator of IFN Regulatory Factor 7.
638 *The Journal of Immunology* **187**, 4754–4763 (2011).
639 61. Q. Zhao, Y. Xie, Y. Zheng, S. Jiang, W. Liu, W. Mu, Z. Liu, Y. Zhao, Y. Xue, J.
640 Ren, GPS-SUMO: A tool for the prediction of sumoylation sites and SUMO-
641 interaction motifs. *Nucleic Acids Res* **42**, W325–W330 (2014).
642 62. J. Ren, X. Gao, C. Jin, M. Zhu, X. Wang, A. Shaw, L. Wen, X. Yao, Y. Xue,
643 Systematic study of protein sumoylation: Development of a site-specific predictor
644 of SUMOsp 2.0. *Proteomics* **9**, 3409–3412 (2009).
645 63. U. Karvonen, T. Jääskeläinen, M. Rytinki, S. Kaikkonen, J. J. Palvimo, ZNF451 Is
646 a Novel PML Body- and SUMO-Associated Transcriptional Coregulator. *J Mol*
647 *Biol* **382**, 585–600 (2008).
648 64. N. Eisenhardt, V. K. Chaugule, S. Koidl, M. Droescher, E. Dogan, J. Rettich, P.
649 Sutinen, S. Y. Imanishi, K. Hofmann, J. J. Palvimo, A. Pichler, A new vertebrate
650 SUMO enzyme family reveals insights into SUMO-chain assembly. *Nature*
651 *Structural & Molecular Biology 2015 22:12* **22**, 959–967 (2015).
652 65. R. J. Lumpkin, H. Gu, Y. Zhu, M. Leonard, A. S. Ahmad, K. R. Clauser, J. G.
653 Meyer, E. J. Bennett, E. A. Komives, Site-specific identification and quantitation of
654 endogenous SUMO modifications under native conditions. *Nature Communications*
655 *2017 8:1* **8**, 1–11 (2017).
656 66. I. A. Hendriks, D. Lyon, D. Su, N. H. Skotte, J. A. Daniel, L. J. Jensen, M. L.
657 Nielsen, Site-specific characterization of endogenous SUMOylation across species
658 and organs. *Nature Communications 2018 9:1* **9**, 1–17 (2018).
659 67. S. Chen, L. C. Francioli, J. K. Goodrich, R. L. Collins, M. Kanai, Q. Wang, J.
660 Alföldi, N. A. Watts, C. Vittal, L. D. Gauthier, T. Poterba, M. W. Wilson, Y.
661 Tarasova, W. Phu, R. Grant, M. T. Yohannes, Z. Koenig, Y. Farjoun, E. Banks, S.

662 Donnelly, S. Gabriel, N. Gupta, S. Ferriera, C. Tolonen, S. Novod, L. Bergelson, D.
663 Roazen, V. Ruano-Rubio, M. Covarrubias, C. Llanwarne, N. Petrillo, G. Wade, T.
664 Jeandet, R. Munshi, K. Tibbetts, M. Abreu, C. A. Aguilar Salinas, T. Ahmad, C. M.
665 Albert, D. Ardissino, I. M. Armean, E. G. Atkinson, G. Atzmon, J. Barnard, S. M.
666 Baxter, L. Beaugerie, E. J. Benjamin, D. Benjamin, M. Boehnke, L. L.
667 Bonnycastle, E. P. Bottinger, D. W. Bowden, M. J. Bown, H. Brand, S. Brant, T.
668 Brookings, S. Bryant, S. E. Calvo, H. Campos, J. C. Chambers, J. C. Chan, K. R.
669 Chao, S. Chapman, D. I. Chasman, R. Chisholm, J. Cho, R. Chowdhury, M. K.
670 Chung, W. K. Chung, K. Cibulskis, B. Cohen, K. M. Connolly, A. Correa, B. B.
671 Cummings, D. Dabelea, J. Danesh, D. Darbar, P. Darnowsky, J. Denny, R.
672 Duggirala, J. Dupuis, P. T. Ellinor, R. Elosua, J. Emery, E. England, J. Erdmann, T.
673 Esko, E. Evangelista, D. Fatkin, J. Florez, A. Franke, J. Fu, M. Färkkilä, K.
674 Garimella, J. Gentry, G. Getz, D. C. Glahn, B. Glaser, S. J. Glatt, D. Goldstein, C.
675 Gonzalez, L. Groop, S. Gudmundsson, A. Haessly, C. Haiman, I. Hall, C. L. Hanis,
676 M. Harms, M. Hiltunen, M. M. Holi, C. M. Hultman, C. Jalas, M. Kallela, D.
677 Kaplan, J. Kaprio, S. Kathiresan, E. E. Kenny, B. J. Kim, Y. J. Kim, D. King, G.
678 Kirov, J. Kooner, S. Koskinen, H. M. Krumholz, S. Kugathasan, S. H. Kwak, M.
679 Laakso, N. Lake, T. Langsford, K. M. Laricchia, T. Lehtimäki, M. Lek, E.
680 Lipscomb, R. J. F. Loos, W. Lu, S. A. Lubitz, T. T. Luna, R. C. W. Ma, G. M.
681 Marcus, J. Marrugat, K. M. Mattila, S. McCarroll, M. I. McCarthy, J. L. McCauley,
682 D. McGovern, R. McPherson, J. B. Meigs, O. Melander, A. Metspalu, D. Meyers,
683 E. V. Minikel, B. D. Mitchell, V. K. Mootha, A. Naheed, S. Nazarian, P. M.
684 Nilsson, M. C. O'Donovan, Y. Okada, D. Ongur, L. Orozco, M. J. Owen, C.
685 Palmer, N. D. Palmer, A. Palotie, K. S. Park, C. Pato, A. E. Pulver, D. Rader, N.
686 Rahman, A. Reiner, A. M. Remes, D. Rhodes, S. Rich, J. D. Rioux, S. Ripatti, D.
687 M. Roden, J. I. Rotter, N. Sahakian, D. Saleheen, V. Salomaa, A. Saltzman, N. J.
688 Samani, K. E. Samocha, A. Sanchis-Juan, J. Scharf, M. Schleicher, H. Schunkert,
689 S. Schönherr, E. G. Seaby, S. H. Shah, M. Shand, T. Sharpe, M. B. Shoemaker, T.
690 Shyong, E. K. Silverman, M. Singer-Berk, P. Sklar, J. T. Smith, J. G. Smith, H.
691 Soininen, H. Sokol, R. G. Son, J. Soto, T. Spector, C. Stevens, N. O. Stitziel, P. F.
692 Sullivan, J. Suvisaari, E. S. Tai, K. D. Taylor, Y. Y. Teo, M. Tsuang, T. Tuomi, D.
693 Turner, T. Tusie-Luna, E. Vartiainen, M. Vawter, L. Wang, A. Wang, J. S. Ware,
694 H. Watkins, R. K. Weersma, B. Weisburd, M. Wessman, N. Whiffin, J. G. Wilson,
695 R. J. Xavier, A. O'Donnell-Luria, M. Solomonson, C. Seed, A. R. Martin, M. E.
696 Talkowski, H. L. Rehm, M. J. Daly, G. Tiao, B. M. Neale, D. G. MacArthur, K. J.
697 Karczewski, A genomic mutational constraint map using variation in 76,156 human
698 genomes. *Nature 2023 625:7993* **625**, 92–100 (2023).
699 68. B. C. Kraemer, T. Schuck, J. M. Wheeler, L. C. Robinson, J. Q. Trojanowski, V.
700 M. Y. Lee, G. D. Schellenberg, Loss of Murine TDP-43 disrupts motor function
701 and plays an essential role in embryogenesis. *Acta Neuropathol* **119**, 409–419
702 (2010).
703 69. Y. Khalfallah, R. Kuta, C. Grasmuck, A. Prat, H. D. Durham, C. Vande Velde,
704 TDP-43 regulation of stress granule dynamics in neurodegenerative disease-
705 relevant cell types. *Sci Rep* **8**, 7551 (2018).
706 70. H. Sidibé, Y. Khalfallah, S. Xiao, N. B. Gómez, H. Fakim, E. M. H. Tank, G. Di
707 Tomasso, E. Bareke, A. Aulas, P. M. McKeever, Z. Melamed, L. Destroimaisons,

J.-E. Deshaies, L. Zinman, J. A. Parker, P. Legault, M. Tétreault, S. J. Barmada, J. Robertson, C. Vande Velde, TDP-43 stabilizes G3BP1 mRNA: relevance to amyotrophic lateral sclerosis/frontotemporal dementia . *Brain*, doi: 10.1093/brain/awab217 (2021).

71. T. A. Shelkovnikova, M. S. Kukharsky, H. An, P. Dimasi, S. Alexeeva, O. Shabir, P. R. Heath, V. L. Buchman, Protective paraspeckle hyper-assembly downstream of TDP-43 loss of function in amyotrophic lateral sclerosis. *Mol Neurodegener* **13**, 1–17 (2018).
72. C. Wang, Y. Duan, G. Duan, Q. Wang, K. Zhang, X. Deng, B. Qian, J. Gu, Z. Ma, S. Zhang, L. Guo, C. Liu, Y. Fang, Stress Induces Dynamic, Cytotoxicity-Antagonizing TDP-43 Nuclear Bodies via Paraspeckle LncRNA NEAT1-Mediated Liquid-Liquid Phase Separation. *Mol Cell* **79**, 443-458.e7 (2020).
73. H. Yu, S. Lu, K. Gasior, D. Singh, S. Vazquez-Sanchez, O. Tapia, D. Toprani, M. S. Beccari, J. R. Yates, S. Da Cruz, J. M. Newby, M. Lafarga, A. S. Gladfelter, E. Villa, D. W. Cleveland, HSP70 chaperones RNA-free TDP-43 into anisotropic intranuclear liquid spherical shells. *Science (1979)* **371** (2021).
74. M. S. Hipp, P. Kasturi, F. U. Hartl, The proteostasis network and its decline in ageing. *Nature Reviews Molecular Cell Biology 2019 20:7* **20**, 421–435 (2019).
75. Y. Gwon, B. A. Maxwell, R.-M. Kolaitis, P. Zhang, H. J. Kim, J. P. Taylor, Ubiquitination of G3BP1 mediates stress granule disassembly in a context-specific manner. *Science (1979)* **372**, eabf6548 (2021).
76. B. A. Maxwell, Y. Gwon, A. Mishra, J. Peng, H. Nakamura, K. Zhang, H. J. Kim, J. P. Taylor, Ubiquitination is essential for recovery of cellular activities after heat shock. *Science (1979)* **372** (2021).
77. M. A. White, E. Kim, A. Duffy, R. Adalbert, B. U. Phillips, O. M. Peters, J. Stephenson, S. Yang, F. Massenzio, Z. Lin, S. Andrews, A. Segonds-Pichon, J. Metterville, L. M. Saksida, R. Mead, R. R. Ribchester, Y. Barhomi, T. Serre, M. P. Coleman, J. R. Fallon, T. J. Bussey, R. H. Brown, J. Sreedharan, TDP-43 gains function due to perturbed autoregulation in a Tardbp knock-in mouse model of ALS-FTD. *Nat Neurosci* **21**, 1138 (2018).
78. A. Dereeper, V. Guignon, G. Blanc, S. Audic, S. Buffet, F. Chevenet, J. F. Dufayard, S. Guindon, V. Lefort, M. Lescot, J. M. Claverie, O. Gascuel, Phylogeny.fr: robust phylogenetic analysis for the non-specialist. *Nucleic Acids Res* **36**, W465–W469 (2008).
79. M. Gertsenstein, L. M. J. Nutter, Engineering Point Mutant and Epitope-Tagged Alleles in Mice Using Cas9 RNA-Guided Nuclease. *Curr Protoc Mouse Biol* **8**, 28–53 (2018).
80. C. J. Miedel, J. M. Patton, A. N. Miedel, E. S. Miedel, J. M. Levenson, Assessment of Spontaneous Alternation, Novel Object Recognition and Limb Clasping in Transgenic Mouse Models of Amyloid-β and Tau Neuropathology. *JoVE (Journal of Visualized Experiments)* **2017**, e55523 (2017).
81. S. J. Guyenet, S. A. Furrer, V. M. Damian, T. D. Baughan, A. R. la Spada, G. A. Garden, A Simple Composite Phenotype Scoring System for Evaluating Mouse Models of Cerebellar Ataxia. *JoVE (Journal of Visualized Experiments)*, e1787 (2010).

82. S. Lê, J. Josse, F. Husson, FactoMineR: An R Package for Multivariate Analysis. *J Stat Softw* **25**, 1–18 (2008).
83. K. Alboukadel, M. Fabian, Extract and Visualize the Results of Multivariate Data Analyses [R package factoextra version 1.0.7] (2020). https://CRAN.R-project.org/package=factoextra.

Acknowledgements:

Human tissue was received from the NIH NeuroBioBank at the University of Maryland, University of Pittsburgh, and Sepulveda sites. The authors also thank all members of the Rousseaux lab for important discussions and critical feedback on the manuscript. The authors also thank the following Core facilities from the University of Ottawa and the Ottawa Hospital Research Institute (OHRI) for use of their facility, equipment, and expertise: the Cell Biology and Imaging Acquisition Core (RRID:SCR_021845), STEMCore Laboratories (RRID:SCR_012601), Genome Engineering and Molecular Biology (GEM) Core (RRID:SCR_022954), Animal Behaviour and Physiology Core (RRID:SCR_022882), Louise Pelletier Histology Core (RRID: SCR_021737), Figs. 1, 2, 4, and S2 were generated in part with Biorender.com.

Funding:

This project was supported in part by an NSERC Discovery Grant and Discovery Launch Supplement to M.W.C.R. (RGPIN-2019-04133 and DGECR-2019-00369); the Canada Research Chairs program to M.W.C.R; the ALS Society of Canada in partnership with the Brain Canada Foundation through the Brain Canada Research Fund, with the financial support of Health Canada, for financial support through the ALS Trainee Award Program 2019 (T.R.S.) and the Discovery Grants Program 2021 (M.W.C.R.); the J.P. Bickell Medical Research Fund (M.W.C.R.); The Eric Poulin Center for Neuromuscular Disease through the Student Translational Research Awards (T.R.S., V.S.G.); The Canadian Institute of Health Research through the CGS-M award (C.E.P., V.S.G.); The Ontario Graduate Scholarship Program Award (C.E.P.); NSERC Undergraduate Summer Research Award (T.T.N.); Medical Student Summer Research Program Award (T.T.N); Christopher Chiu senior postdoctoral fellowship (P.M.M.); James Hunter and Family ALS Initiative (J.R.).

Author Contributions

Conceptualization: TRS, CEP, MWCR

Methodology: TRS, CEP, TTN, JLZ, VSG, PMM, BN, PMM, SMC, JLR

Investigation: TRS, CEP, TTN, JLZ, MMH, ACG, VSG, PMM, BN, JLR

Visualization: TRS, CEP, MWCR

Funding acquisition: TRS, CEP, MWCR

Project administration: JMW, JR, MWCR

Supervision: JR, MWCR

Writing – original draft: TRS, MWCR

Writing – review & editing: TRS, MWCR

Competing interests: Authors declare that they have no competing interests.

Data and materials availability: All data are available in the main text or the supplementary materials.

Supplementary Materials

Materials and Methods
Figs. S1-S11
Tables S1-S5

Figure Captions

Fig. 1: SUMOylation dynamically regulates nuclear TDP-43 in a stress-responsive manner. (A) Schematic of immunoprecipitation assays to detect TDP-43 SUMOylation. **(B)** Representative SUMOylation Assay western blot detecting TDP-43 SUMOylation specifically in response to 1 hour sodium arsenite (250 µM) stress. * = SUMOylated TDP-43, ** = PolySUMOylated TDP-43. **(C)** Representative image and quantification of relative proximity ligation signal between TDP-43 and SUMO2/3 in murine primary cortical neuron cultures in response to 1 hour sodium arsenite (250 µM) treatment. Scalebar = 20 um. (N = 4 per condition) Unpaired T-test, *** $p<0.0005$ **(D)** Representative GFP-Trap SUMOylation assay depicting increased SUMOylation with ALS-causing Q331K mutation and blocked SUMOylation by disruption of the Nuclear Localization Sequence (NLS^{mut}) in response to 250 µM sodium arsenite stress. **(E)** Representative SUMOylation Assay of TDP-43 SUMOylation dynamics during stress (250 µM sodium arsenite) and recovery demonstrating a dependency on the ubiquitin proteosome for clearance of polySUMOylated TDP-43 by treatment with proteasome inhibitor MG132 (2uM). **(F)** Representative GFP-Trap SUMOylation assay screening for potential E3 ligases regulating TDP-43 SUMOylation in response to 1 hour sodium arsenite stress (250 µM). (N = 3) RM One-Way ANOVA with Fisher's LSD test, * $p<0.05$, ** $p<0.005$, *** $p<0.0005$, **** $p<0.0001$.

Fig. 2: Blocking TDP-43 SUMOylation at conserved K408 impairs the cellular stress response. (A) Representative GFP-Trap SUMOylation assay to map the site of TDP-43 SUMOylation in response to 1 hour sodium arsenite (250 µM) stress. **(B)** Phylogenetic representation from alignment of representative TDP-43 paralogs highlighting the emergence and conservation of [human] K408 (Blue). **(C)** Pairwise identity of the [human] TDP-43 C-terminal domain from MUSCLE alignment of 300 amino acid sequences for TDP-43 paralogs from Humans to Actinopterygii from OrthoDB. Red represents the TDP-43 C-terminal domain (Intrinsically disordered domain). Cyan represents PTM- enriched region at the extreme C-terminus. **(D)** Representative GFP-Trap SUMOylation assay with phospho-dead TDP-43 "4SA" (S403/404/409/410A) highlighting antagonism between SUMOylation and phosphorylation. **(E)** Schematic and sanger sequencing of the TDP-43^{K408R} knock in mouse line. **(F)** Representative images and quantification of G3BP1 stress granule dynamics and TDP-43 nuclear foci formation in mouse primary cortical neurons (7 DIV) during stress (1 hour 250 µM sodium arsenite) and

835 recovery. Cyan arrowheads denote cells with nuclear TDP-43 foci, magenta arrow in insets
836 denote TDP-43 foci. G3BP1 contrast was set for optimal visualization of stress granules. Scale
837 Bar = 25 µm. N=5, 2-Way ANOVA with Fisher's LSD test, ** p<0.005. **(G)** Representative
838 western blot and quantification of RIPA and UREA fractions from mouse primary cortical
839 neurons (7 DIV) during stress (1 hour 250 µM sodium arsenite) and recovery. N=3-5, 2-Way
840 ANOVA with Fisher's LSD test, * p<0.05, ** p<0.005.

841

842 **Fig. 3: Blocking TDP-43 SUMOylation *in vivo* leads to sex-specific and age-dependent**
843 **impairment and pathology. (A)** Representative image of a barbered female mouse and
844 quantification of cumulative barbering probability. 2-Way ANOVA with Tukey's Multiple
845 Comparisons, *** p<0.0005. **(B)** Tube test of social dominance in female mice 16 months of age
846 (16MO) displaying the total head-to-head battles and win percentage by genotype comparing
847 Wild Type against K408R (K408R/+ and K408R/K408R animals). Binomial Test of Observed
848 vs. Expected with Expected due to random chance set to 50%, * p<0.05. **(C)** Quantification of
849 total distance traveled (cm) and total time in center (s) of female mice in the open field test.
850 Mixed Effects Analysis with Tukey's multiple comparison, *** p<0.0005, * p<0.05. **(D)**
851 Quantification of percent alternations in the spontaneous Y-maze test in female mice at 2, 9, and
852 16 months of age (2MO, 9MO, 16MO, respectively). Mixed-Effects Analysis with Tukey's
853 multiple comparison, * p<0.05. (E) Quantification of relative ambulatory activity normalized to
854 Wild Type at 1 hour in female mice at 2, 9, and 16 months of age (2MO, 9MO, and 16MO,
855 respectively). Grey shading between hours 2 and 14 indicate "lights off" with respect to
856 day/night light cycle. 2-Way ANOVA with Tukey's multiple comparison, * p<0.05. **(F)**
857 Representative images and quantification of TDP-43 mislocalization in the lumbar spinal cord of
858 9-month-old TDP-43^{K408R} mice. Each datapoint represents the average of 4 serial sections 40 µm
859 apart per individual mouse. Scalebar = 100 µm. (N = 8 per genotype, 4 per sex/genotype)
860 Unpaired t-test, *** p<0.0005. See fig. S10A for sex comparisons. **(G)** Representative images
861 and quantification of neuromuscular junction (NMJ) innervation in the tibialis anterior of 16-
862 month-old male TDP-43^{K408R} mice. Scale bar = 30 µm. (N = 4 per genotype) 2-Way ANOVA
863 with Tukey's multiple comparison analysis, *p<0.05, ****p<0.0001.

864

865 **Fig. 4: SUMOylation correlates with aging and is enriched in the prefrontal cortex of**
866 **ALS/FTD patients.** (A) Demographic composition of temporal lobe samples from aging cohort.
867 (B) Representative western blot and box plot of SUMO2/3 across binned age groups. Average
868 Age: "Young" = 6.32 yrs, N = 14; "Adult" = 31.11 yrs, N = 20; "Aged" = 64.00 yrs, N = 19.
869 Error bars indicate 10-90 percentile. Kruskall-Wallis with Uncorrected Dunn's multiple
870 comparisons test. * p<0.05, ** p<0.005. (C) Representative images and quantification from
871 proximity ligation assay (PLA) between SUMO2/3 and TDP-43 in the prefrontal cortex.
872 Unaffected patient ID: NP23-02, Female, 74 yrs. ALS/FTD patient ID: A14-101, Female, 67 yrs.
873 Scale bar = 25 µm. (N = 7-8) Unpaired T-test, * p<0.05.

874

875 **Supplemental Figure Captions**

876 **fig. S1: Characterizing stress responsive TDP-43 SUMOylation. (A)** Representative western
877 blot from SUMOylation assays testing whether various stressors that cause TDP-43 aggregation

878 induce TDP-43 SUMOylation: NaAsO2 (250 μM), D-Sorbitol (400 mM), NaCl (300 mM), Heat
879 Shock (42 °C). **(B)** Representative western blot from SUMOylation assays testing the selectivity
880 of SUMO paralogs to SUMOylate TDP-43 in response to 1 hour sodium arsenite (250 μM)
881 stress. **(C)** Representative images of SUMO2/3 and TDP-43 in the nucleus of mouse cortical
882 motor neurons (7 DIV) in unstressed and 1 hour sodium arsenite (250μM) stressed conditions.
883 **(D)** Representative control imaged from Proximity Ligation Assay (PLA) in mouse primary
884 cortical neurons. Scalebar = 20 μm. (N = 4). **(E)** Representative western blot and quantification
885 from GFP-Trap SUMOylation assays testing the kinetics of TDP-43 SUMOylation in response to
886 sodium arsenite stress (250 μM) and its relationship to insoluble phosphorylated TDP-43. (N =
887 3) **(F)** Representative dose-response assay to detect TDP-43 SUMOylation after 1 hour of
888 sodium arsenite stress (1 = 250 μM, 1/2 = 125 μM, 1/4 = 62.5 μM, etc.)

889 **fig. S2: Generation of the TDP-43^{K408R} mouse line. (A)** Schematic of the knock in approach to
890 edit the endogenous *Tardbp* to express TDP-43^{K408R}. **(B)** Schematic of LNA probe based
891 genotyping approach and allelic discrimination assay to genotype TDP-43^{K408R} mouse line. **(C)**
892 Sex and mendelian ratios of F3 generation TDP-43^{K408R} mice from K408R/+ and K408R/+
893 breeding pairs used to generate behavior and histology cohorts. Observed vs Expected statistical
894 analysis assuming an expected 1:1 ratio sex ratio and 1:2:1 mendelian ratio.

895 **fig. S3: Characterizing the stress response in TDP-43^{K408R} primary cortical neuron**
896 **cultures. (A)** Classification and quantification of G3BP1 stress granule (SG) intensity in
897 response to 1 hour sodium arsenite stress (250 μM) and recovery. (N = 5 per genotype) 2-Way
898 ANOVA with Tukey's multiple comparisons analysis. *p<0.05, ***p<0.0005. **(B)**
899 Quantification of the localization of G3BP1 stress granules (SGs) in response to 1 hour sodium
900 arsenite stress (250 μM) and recovery. (N = 5 per genotype) 2-Way ANOVA with Tukey's
901 multiple comparisons analysis. ***p<0.0005. **(C)** Quantification of the percentage of neurons
902 with positive TDP-43 nuclear foci in G3BP1 stress granule positive and G3BP1 stress granule
903 negative neurons in response to 1 hour sodium arsenite stress (250 μM) and recovery. (N = 5 per
904 genotype) 2-Way ANOVA with Tukey's multiple comparisons analysis. ***p<0.0005. **(D)**
905 Quantification of the average number of TDP-43 nuclear foci in neurons positive for TDP-43
906 nuclear foci in response to 1 hour sodium arsenite stress (250 μM) and recovery. (N = 5 per
907 genotype) 2-Way ANOVA with Tukey's multiple comparisons analysis. *p<0.05.

908 **fig. S4: Characterization of TDP-43^{K408R} during development. (A)** Genotype and sex
909 composition of mice subject to behavior testing. **(B)** Weight of mice at P10-P11. Unpaired T-test
910 (Males); Mann-Whitney test (Females and All) **(C)** Quantification of the duration hanging on a
911 wire at P10-P11. Mann-Whitney test (Males, Females, and All). **(D)** Survival curve for male and
912 female TDP-43^{K408R} mice. Curve comparisons analyzed using Log-Rank test and Gehan-
913 Breslow-Wilcoxon test. **(E)** Weights of male and female TDP-43^{K408R} mice from 3 weeks to 64
914 weeks of age. Mixed-effects analysis. **(F)** Hindlimb clasping scores of male and female TDP-
915 43^{K408R} mice from 3 weeks to 64 weeks of age. Mixed-effects analysis. See table S2 for raw data
916 details on statistical tests.

917 **fig. S5: Characterizing the cognitive and social behavior of TDP-43^{K408R} mice.**
918 Quantification of cognitive and social behaviors in the **(A)** Light/Dark Box, **(B)** Y-maze, **(C)** 3
919 Chamber Social Interaction, **(D)** Marble Burying, and **(E)** Tail Suspension behavior tasks at 2, 9,
920 and 16 months of age (2MO, 9MO, and 16MO, respectively) in male and female TDP-43^{K408R}
921 mice. All behavior tests were analyzed with a Mixed-Effects Model with Tukey's multiple
922 comparison analysis, see table S2.

923 **fig. S6: Characterizing the motor behavior of TDP-43^{K408R} mice.** Quantification of motor
924 abilities in the **(A)** Hanging Wire, **(B)** Grip Strength, and **(C)** Rotarod behavior tasks at 2, 9, and
925 16 months of age (2MO, 9MO, and 16MO, respectively) in male and female TDP-43^{K408R} mice.
926 Behavior tests were analyzed with 2-Way ANOVA or Mixed-Effects Models, see table S2.

927 **fig. S7: Digigait analysis of TDP-43^{K408R} mice.** Principle component analyses of all outputs
928 from the Digigait behavior test for male and female TDP-43^{K408R} mice at 2, 9, and 16 months of
929 age (2MO, 9MO, and 16MO, respectively).

930 **fig. S8: Characterizing the activity of TDP-43^{K408R} mice.** Quantification of **(A)** total distance
931 traveled (cm) and time in center (s) during the Open Field behavior test and **(B)** the relative
932 ambulatory activity (males) of TDP-43^{K408R} mice at 2, 9, and 16 months of age (2MO, 9MO, and
933 16MO, respectively). Behavior tests were analyzed with 2-Way ANOVA or Mixed-Effects
934 models, see table S2.

935 **fig. S9: Molecular characterization of TDP-43^{K408R} mice. (A)** Representative western blot and
936 quantification of TDP-43 and phosphorylated TDP-43 in the RIPA and UREA fractions of the
937 cortex from male mice at 2, 9, and 16 months of age (2MO, 9MO, and 16MO, respectively. N =
938 4 per genotype) 2-Way ANOVA with Fisher's LSD test. **(B)** Representative western blot and
939 quantification of TDP-43 and phosphorylated TDP-43 in the RIPA and UREA fractions of the
940 cortex from male mice at 2, 9, and 16 months of age (2MO, 9MO, and 16MO, respectively). (N
941 = 4 per genotype) 2-Way ANOVA with Fisher's LSD test, *p<0.05, **p<0.005, ***p<0.0005.
942 **(C)** Representative western blot and quantification of TDP-43 and phosphorylated TDP-43 in the
943 RIPA and UREA fractions of the lumbar spinal cord at 2, 9, and 16 months of age (2MO, 9MO,
944 and 16MO, respectively. N = 8 per genotype; 4 per sex/genotype) 2-Way ANOVA with Fisher's
945 LSD test, *p<0.05, ***p<0.0005, ****p<0.0001.

946 **fig. S10: Histological characterization of TDP-43^{K408R} lumbar spinal cord. (A)**
947 Quantification of TDP-43 mislocalization in the lumbar spinal cord of 9-month-old from Fig. 3F
948 split by sex. Each datapoint represents the average of 4 serial sections 40 µm apart from an
949 individual mouse. Unpaired t-test. * = p<0.05, ** = p<0.005. **(B)** Representative images and
950 quantification of ChAT+ motor neurons in the ventral horn of the lumbar spinal cord of male and
951 female mice. Each datapoint is the average of 4 serial sections spaced 40 µm apart through the
952 lumbar enlargement of the lumbar spinal cord. Unpaired t-test, ** p<0.005. **(C)** Example images
953 of neuromuscular junctions (NMJs) for scoring criteria to assess fully innervated, partially
954 innervated, and fully denervated NMJs.

955 **fig. S11: Optimization of proximity ligation assay in human tissue.** Representative images of
956 proximity ligation assay (PLA) between TDP-43 and SUMO2/3 in human PPFE hippocampus
957 tissue sections (5um). Yellow arrows indicate TDP-43:SUMO2/3 interactions where the signal
958 specific to the PLA channel and not identified in the autofluorescence channel. Scalebar = 18
959 µm.

960

961 **Materials and Methods**

962 ***Cloning of pEGFP-TDP-43 plasmid and variants***

963 For expression of C-terminally tagged TDP-43-EGFP, human TDP-43 was subcloned out of a
964 wtTDP-43tdTOMATOHA (gift from Zoushang Xu, Addgene # 28205) via XhoI and Kpn1
965 double digest and inserted into a pEGFP-N3 (Clontech) backbone and validated by sanger

966 sequencing. Site directed mutagenesis was performed using QuikChange II XL (Agilent 200521)
967 following manufacturer instructions. Primers for site directed mutagenesis can be found in table
968 S4. Several TDP-43 variants were generated through the uOttawa Genome Engineering and
969 Molecular Biology facility or designed and ordered through twist bioscience and were subcloned
970 into the pEGFP-TDP-43 backbone for consistency using XhoI and HindIII double digest, see
971 table S4 for plasmids used/generated in this study.

972 ***Generation of pL302-HA-SUMO2 stable HEK293T cell line***

973 To generate a pL302-HA-SUMO2 lentivirus-compatible vector for stable HA-SUMO2
974 expression, HA-SUMO2 was subcloned from pcDNA-HA-SUMO2 (gift from Guy Salvesen,
975 Addgene #48967) and inserted into the pL302 lentiviral backbone (gift from Jacqueline Burré
976 and Thomas Südhof at Stanford). Briefly, extension PCR was performed to add an Xba1
977 restriction site to the 5' and 3' ends of the HA-SUMO2 insert using PCR amplification using
978 forward primer sequence*: 5'- ggctgcaggtcgactctagaaagcttatggatgcctaccc-3'*, and reverse primer
979 sequence*: 5'- tggctgcaggtcgactctagatgcatgctcgagtcaacct-3'.* The PCR amplicon and pL302
980 backbone were digested with XbaI and the amplicon was ligated into the pL302 backbone.
981 Colonies were screened by sanger sequencing to ensure proper orientation and copy number of
982 the insert. Next the pL302-HA-SUMO2 plasmid was packaged into lentivirus by co-transfection
983 of psPAX2 (Gift from Didier Trono, Addgene #12259), and pMD2-G (Gift from Didier Trono,
984 Addgene #12260) into HEK293T cells and subsequent media collections. Viral media was
985 filtered through a 0.45 µm filter then concentrated by centrifugation at 100,000G for 2 hours at 4
986 °C and the pellet was resuspended in 1X PBS. Fresh HEK293T cells were transduced with
987 pL302-HA-SUMO2 virus to generate a stable polyclonal cell line.

988 ***GFP-trap SUMOylation assay***

989 ~250,000 HEK293T and/or pL302-HA-SUMO2 HEK293T cells were seeded (experiment
990 dependent) in a 6-well plate. The following day, plasmids were transfected to express TDP-43-
991 GFP (or mutant variants) and/or HA-SUMO variants and allowed to incubate for 48 hours for
992 optimal expression. Cells were treated with 250 µM $NaAsO_2$ for one hour (or variations of time,
993 concentration, or chemical depending on assay), after which cells were immediately collected by
994 scraping the bottom of the well and pelleting the samples by centrifugation at 2500G for 5 minutes
995 at room temperature. The supernatant was then aspirated, and the cells were flash frozen or
996 immediately lysed in 450 uL of ice cold 1X Denaturing Lysis buffer (1X RIPA, supplemented
997 with 1X protease inhibitor, 1X phosphatase inhibitor, 50mM N-Ethylmalamide, and 5% 2-
998 mercaptoethanol) and boiled at 95 °C for 5 minutes. After boiling, 450 uL of ice cold 1X Lysis
999 buffer (1X RIPA, supplemented with 1X protease inhibitor, 1X phosphatase inhibitor, 50mM N-
1000 Ethylmalamide) was then added to the sample, and cells were left on ice for 20 minutes with
1001 vortexing every 5 minutes for 10 second. Next, the cell lysates are centrifuged at ~21000G for 20
1002 minutes at 4 °C and during this time, 30 uL of GFP-Trap beads (Bulldog Bio) per sample were
1003 washed 3 times in cold 1X RIPA buffer then aliquoted equally into microcentrifuge tubes for each
1004 sample. Following the centrifugation, 1-3% of the supernatant was transferred into a
1005 microcentrifuge tube to be used as the *Input* sample. The remainder of the supernatant was
1006 transferred into a microcentrifuge tube containing the GFP-Trap beads as the immunoprecipitation
1007 sample and was then placed on a rotator for 45 minutes at 4 °C. After the incubation, the solution
1008 was aspirated, and the beads were washed using cold 1X RIPA buffer 5 times. Samples were eluted
1009 in 2X Laemmli buffer containing 10% Beta-Mercaptoethanol and boiled at 85 °C for 10 minutes
1010 at 1250 rpm on a thermomixer. The input samples were prepared with 4X Laemmli buffer

1011 containing 10% Beta-Mercaptoethanol and then boiled at 85 °C for 10 minutes. Samples were then
1012 analyzed by Western Blot.

1013 ***Endogenous SUMOylation assay***

1014 ~500,000 HEK293T and/or pL302-HA-SUMO2 HEK293T cells were seeded (experiment
1015 dependent) in a 6-well plate. The following day, cells were treated respective of their experiment
1016 after which cells were immediately collected by scraping the bottom of the well and pelleting the
1017 samples by centrifugation at 2500G for 5 minutes at room temperature. The supernatant was then
1018 aspirated, and the cells were flash frozen or immediately lysed in 100 uL of 1% SDS buffer (1%
1019 SDS in IP Lysis Buffer supplemented with 1X protease inhibitor, 1X phosphatase inhibitor,
1020 100mM N-Ethylmalamide), vortexed for 20 seconds then boiled at 95C for 10 minutes. After
1021 boiling, 900 µL of ice-cold IP Lysis buffer was then added to the sample, and cells were left on
1022 ice for 20 minutes with vortexing every 5 minutes for 10 second. Next, the cell lysates are
1023 centrifuged at ~21000G for 20 minutes at 4 C. Following the centrifugation, 1-3% of the
1024 supernatant was transferred into a microcentrifuge tube to be used as the *Input* sample. The
1025 remainder of the supernatant was transferred into a microcentrifuge tube containing 1 to 10 ug of
1026 antibody per sample (See table S5 for concentrations) and incubated overnight rotating at 4 °C.
1027 The next day, the solution was added to a magnetic rack kept at 4 °C and the supernatant was
1028 collected for *flowthrough* to test immunodepletion or aspirated. The beads were washed 5X in ice
1029 cold IP Lysis buffer. Samples were eluted using 5 ug of synthetic HA peptide (Sino Biological)
1030 per 1ug of antibody and incubating at 37 °C for 15 minutes at 900rpm on a thermomixer (for anti-
1031 HA immunoprecipitations) or by boiling in 2X Laemmli buffer containing 10% Beta-
1032 Mercaptoethanol at 85C for 10 minutes at 1250rpm on a thermomixer (for other endogenous
1033 immunoprecipitations). The input/flowthrough and HA immunoprecipitation samples were
1034 prepared with 4X Laemmli buffer containing 10% Beta-Mercaptoethanol and then boiled at 85 °C
1035 for 10 minutes. Samples were then analyzed by Western Blot using light chain specific secondary
1036 antibodies.

1037 ***Serial protein extraction from cell culture***

1038 Soluble protein was extracted using RIPA buffer (supplemented with protease inhibitor,
1039 phosphatase inhibitor, and 50mM N-Ethylmalamide) during immunoprecipitation assays (taken
1040 as *Input* prior to immunoprecipitation) or from lysate in cortical neuron experiments. The
1041 remaining pellet after the centrifugation step post-lysis was washed in 1mL RIPA buffer with
1042 vortexing for 10 seconds followed by centrifugation at ~21000G for 20 minutes at 4 °C. The
1043 supernatant was carefully removed, and the pellet was resuspended in 300 µL of 2% SDS buffer
1044 in PBS for immunoprecipitation assays, or in 300 µL of 8M UREA in PBS with 10mM Tris-HCl
1045 pH 7.4. Samples were left to solubilize overnight at room temperature before 2X Laemmli was
1046 added prior to Western Blot analysis.

1047 ***Western blot analysis***

1048 Protein sample prepared in Laemmli loading buffer was loaded onto 8% polyacrylamide gel,
1049 TGx Mini-PROTEAN 4-15% precast gel (BioRad), or Bolt Bis-Tris Plus mini-Protein Gel 4-
1050 12% (Invitrogen) and run at 100-140 constant voltage in Tris-Glycine or MES buffer for their
1051 respective gels. Proteins were transferred onto a 0.45 µm nitrocellulose membrane at a constant
1052 340 mA for 2 hours at 4 °C. The membranes were blocked in 10% milk diluted in TBS-T,
1053 washed 5 x 5 minutes in TBS-T then incubated in primary antibody overnight (table S5). The
1054 following day the membranes were washed for 5 x 5 minutes in TBS-T, then incubated in

1055 secondary antibody for 1-2 hours at room temperature. Finally, the secondary antibody is washed
1056 5 x 5 minutes in TBS-T before being imaged using chemiluminescence Clarity Western ECL or
1057 Clarity Max Western ECL on an LAS4000 (GE). Densitometry was performed using the
1058 volumes function of the ImageLab (BioRad) software.

1059 ***Conservation analysis of TDP-43 K408***

1060 Representative FASTA amino acid sequences of TDP-43 paralogs were aligned for phylogenetic
1061 analysis using MUSCLE multiple alignment and PhyML maximum likeliness for phylogenetic
1062 tree generation(*78*). Pairwise alignment of the C-terminal domain was performed using Geneious
1063 Prime 2022.1.1 (https://geneious.com) performing a MUSCLE multiple alignment of 300 FASTA
1064 amino acid sequences of TDP-43 paralogs between Humans and Actinopterygii representing the
1065 emergence of [human] K408 curated from the OrthoDB database (table S1).

1066 ***Mouse lines***

1067 *C57BL6/N, TDP-43^{K408R} (C57BL6/N Background)*

1068 ***Sex and age of experimental mice***

1069 Experiments were performed using both male and female mice sufficiently powered to detect sex
1070 differences. In some instances where no sex differences were observed, male and female mice
1071 were grouped together to assess genotypic differences independent of sex. Experiments
1072 involving primary cortical neurons cultures dissected from individual embryos were used
1073 involving a mixture of male and female embryos. Experimental animals underwent behavioral
1074 testing as early as P10 and as late as 16 months of age. See table S2 for raw data and statistical
1075 analyses.

1076 ***Mouse husbandry***

1077 All mouse procedures were carried out in accordance with the Canadian Council on Animal Care
1078 and approved by the University of Ottawa Animal Care Committee. All mice were group housed
1079 (3-5 per mice cage) with access to food and water *ad libitum* on a standard 12-hour light dark
1080 cycle. Exceptions included adult male mice who were separated and single housed if persistent
1081 fighting and fight wounds were observed in the cage. All experimental mice were given crinkle
1082 paper in addition to the standard nestlet and hut enrichment material. Husbandry was completed
1083 by University of Ottawa Animal Care and Veterinary Services except for cohorts actively
1084 undergoing behavior testing for which husbandry was completed by the experimenter.

1085 ***TDP-43^{K408R}* mouse line generation**

1086 At The Centre of Phenogenomics (SickKids, Toronto, ON, Canada), the *TDP-43^{K408R}* mice were
1087 generated on a C57BL6/N background based on previous methods (*79*) using CRISPR/Cas9-
1088 mediated gene editing of the endogenous *Tardbp* locus. In brief, spCas9 loaded with an sgRNA
1089 to target exon 6 of *Tardbp (MGI:2387629; 5'-TGGGGGCTTTGGCTCGAGCA-3')* was
1090 electroporated into embryos alongside a single stranded oligonucleotide (ssODN) repair template
1091 (5'-
1092 C*TAAATCTACCTAACCTAATAACCAACCTACTAACCACCCCCCACCACCTACATTCCCCAG*
1093 *CCAGAAGAC**c**TAGAATCCATG**ga**CGAGCCAAAGCCCCCATTAAAACCACTGCCCGATCCTG*
1094 *CATTTGATGCTGACCCCCAACCAAGGGGGGC-3'*). Embryos were screened via allelic
1095 discrimination (see "TDP-43^{K408R} genotyping" below) to identify founders. Four founders were
1096 crossed to C57BL6/N mice to ensure germline transmission of knock-in allele.

1097 ***TDP-43^{K408R} genotyping***

1098 Tail samples were collected prior to weaning and again postmortem for genomic DNA (gDNA)
1099 isolation and genotyping. Tails were solubilized in 300 µL solubilization buffer (10X SET, 100
1100 mM NaCl, 100 µg/mL Proteinase K (Bio Basic PB0451-250)) at 55 °C overnight. Cell debris
1101 was precipitated by adding 150 µL of "Tail Salts Buffer" (4.31M NaCl, 0.63M HCl, 10 mM
1102 Tris-HCl, pH7.4) then samples were centrifuged at ~21,000*g* for 15 minutes at 4 °C. Supernatant
1103 containing gDNA was transferred into 600 µL of chilled 100% ethanol to precipitate nucleic
1104 acids which were then pelleted by centrifugation for 10 minutes at ~21,000*g* at 4 °C. The
1105 supernatant was carefully removed, and the pellet was washed in 600 µL of chilled 70% ethanol
1106 then centrifuged at ~21,000*g* at 4 °C for 5 minutes. The supernatant was carefully removed, and
1107 residual supernatant was left to evaporate for 5 minutes. The gDNA pellet was resuspended in
1108 double distilled H2O at 55 °C for 10 minutes. Genotyping reaction was prepared in a 10 µL
1109 reaction containing ~5ng of gDNA, 250nM *K408R Genotyping Forward* primer (5'-
1110 *CCACCATTCTAAATCTACCTAACCTAATA-3'*), 250nM *K408R Genotyping Reverse* primer (5'-
1111 *GGATCGGGCAGTGGTTTTA-3'*), 125nM Wild Type Locked Nucleic Acid (LNA) probe (*HEX-*
1112 *TCT+A+A+GT+CT+TCT+GGC-IowaBlack FQ),* 125nM K408R LNA probe (*FAM-*
1113 *TCT+A+G+GT+CT+T+CT-IowaBlack FQ),* and 2X PerfeCTa qPCR Tough Mix (QuantaBio).
1114 Reactions were run on a BioRad CFX96 qPCR thermocycler with the following cycling
1115 parameters: Initial annealing at 95 °C for 2 minutes, followed by 40 cycles of 95 °C for 15
1116 seconds then 60 °C for 60 seconds. Results were analyzed via allelic discrimination in the
1117 BioRad Maestro software. See fig. S2B.

1118 ***Mouse wellness monitoring***

1119 Mice were monitored weekly starting at age P21 and included assessment of hindlimb clasping,
1120 kyphosis, weight, and general health. The hindlimb function was assessed following previous
1121 methods (*80*). Briefly, the mouse was suspended in the air for approximately 5-10 seconds by the
1122 base of the tail. Features of the limbs were assessed to give a score from 0-4. Kyphosis was
1123 assessed by allowing the mice to briefly walk on the flat table top in the housing room and
1124 visually observing the straightness of the spine. A score of 0-3 was given based on previously
1125 described methods(*81*). Weight was measured every other week by placing individual mice on a
1126 digital weigh scale. Notably, mice exhibiting barbered patches were monitored and recorded.

1127 ***Primary cortical neuron cultures***

1128 Pregnant mice were euthanized between gestation E13.5–15.5 with 120 mg/kg Pentobarbital
1129 Sodium (Bimeda-MTC, 8015E) delivered via intraperitoneal injection. The embryos were
1130 removed and placed into ice cold 1X PBS. For each embryo, the cortices were carefully isolated
1131 and meninges removed and then placed in ice cold HBSS (Sigma Aldrich). Cortices were
1132 dissociated for 20 minutes with trypsin (Thermo Scientific) at room temperature on a rotator
1133 before trypsin inhibitor with DNase solution was added to quench the reaction. Cells were
1134 pelleted at 2,500 x *g* for 5 minutes at 4°C. The supernatant was carefully removed and the pellet
1135 was washed with trypsin inhibitor plus DNase solution. Cortical neurons were pelleted at 2,500
1136 x *g* for 5 minutes at 4°C. The supernatant was carefully removed and the neurons were
1137 resuspended in 1 mL of ice cold outgrowth media (Neurobasal media (Thermo Scientific),
1138 supplemented with 1X B-27 (Thermo Scientific), 1X N-2 (Thermo Scientific), 500 µM L-
1139 Glutamine (Wisent Bioproducts), and 0.5% penicillin/streptomycin (GE Healthcare Life
1140 Sciences)). Culture dishes and coverslips were prepared in advanced coated with 50 µg/mL Poly-

1141 D-Lysine overnight at 37 °C specific to each experiment detailed below. Cultures were
1142 maintained for 7-9 days *in vitro* prior (DIV) to experimentation.

1143 ***Immunofluorescence in primary cortical neurons***

1144 Micro Coverglass #1.5 coverslips (Electron Microscopy Sciences) coverslips were washed in 2M
1145 HCl overnight at 55 °C, washed 5 times in sterile H_2O, then pre-coated with poly-D-lysine
1146 (50 µg/mL) overnight at 37 °C, then washed with distilled water three times and air-dried at
1147 room temperature for at least 2 hours. Primary mouse cortical neurons were seeded at 75,000-
1148 100,000 cells per coverslip and cultured as described above. On day 7, neurons were fixed for 10
1149 minutes using 10% phosphate buffered formalin for (Fisher Chemical, SF100-4) followed by 3 x
1150 5-minutes washes in 1 mL of 1X PBS. Neurons were blocked in 500 µL of blocking buffer (1%
1151 Triton X-100, 10% cosmic calf serum in 1X PBS) for 1 hour, then incubated in 300 µL of
1152 primary antibody diluted in blocking buffer overnight at 4 °C. The following day, the neurons
1153 were washed for 5 x 5-minutes in 1 mL of 1X PBS then incubated in 300 µL of secondary
1154 antibody diluted in blocking buffer for 2 hours at room temperature. Neurons were then washed
1155 in 1 mL 1X PBS, then stained with DAPI for 10 minutes at room temperature followed by 4 x 5-
1156 minutes washes in 1X PBS before being mounted using antifade fluorescence mounting media
1157 (Dako, S3023).

1158 ***Proximity ligation assay in primary cortical neurons***

1159 Primary mouse cortical neurons were cultured and fixed as described in *primary cortical neuron*
1160 *cultures* and *immunofluorescence in primary cortical neurons*. Fixed coverslips were transferred
1161 into 12-well plates and outlined with a hydrophobic pen and blocked using 40 µL of Duolink
1162 blocking buffer (Sigma Aldrich, DUO82007) at 37 °C for 1 hour. Coverslips were then washed
1163 for 3 × 5 minutes in 1 mL 1X PBS. Next, coverslips were incubated in 300 µL of primary
1164 antibody (anti-TDP-43 1:750, PTGLabs; anti-SUMO2/3 [8A2] 1:500 Sigma) diluted in blocking
1165 buffer (1.5% Triton X-100, 10% cosmic calf serum in 1X PBS) overnight at 4 °C. The next day,
1166 the coverslips were washed for 3 × 5 minutes in 1 mL of Duolink Wash Buffer A (0.01 M Tris-
1167 Base, 0.15 M NaCl, 0.05% Tween-20, pH 7.4) followed by incubation at 37°C for 1 hour in
1168 40 µL of dilute probe mixture containing a 1:5 dilution of Duolink PLA MINUS (Sigma Aldrich,
1169 DUO82004) and PLUS probes (Sigma Aldrich, DUO82002) in antibody diluent (Sigma Aldrich,
1170 DUO82008). Duolink PLA probes were diluted in antibody diluent (Sigma Aldrich, DUO82008)
1171 at a 1:5 dilution. Coverslips were washed for 3 × 5 minutes in Duolink Wash Buffer A and then
1172 incubated in 40 µL of ligase (Sigma Aldrich, DUO82027) diluted in 1X ligation buffer (Sigma
1173 Aldrich, DUO82009) at a 1:40 dilution at 37 °C for 30 minutes. The coverslips were then
1174 washed for 3 x 5-minutes washes in Duolink Wash Buffer A and then incubated in 40 µL of
1175 polymerase (Sigma Aldrich, DUO82028) diluted 1:80 in 1X amplification buffer (Sigma
1176 Aldrich, DUO82011) at 37°C for 90 minutes. Next, the coverslips were washed 2 × 10 minutes
1177 in Duolink Wash Buffer B (0.2 M Tris-Base, 0.1 M NaCl, pH 7.5) and then again in 1 mL of
1178 Duolink Wash Buffer B diluted at 1:100 in 1X PBS for 1 minute. Coverslips were briefly air
1179 dried and then mounted on slides using Vectashield Antifade Mounting Medium with DAPI. Z-
1180 stack images were obtained on a Zeiss AxioObserverZ1 LSM800 Confocal Microscope at 63×
1181 magnification with a 5× digital zoom through a Z distance of 10-12 µm per image using optimal
1182 0.27 µm spacing per slice with dimensions set to 512 × 512 pixels with 2X averaging per frame.
1183 ~5 images were randomly obtained around the coverslip sampling >15 cells per condition per
1184 replicate. Images were analyzed and quantified using the Spots function on the Imaris (ver. 9.9.1
1185 Bitplane, Switzerland) software.

1186 ***Cell viability in primary cortical neurons***

1187 Mouse primary cortical neurons were collected and cultured as described in "Primary cortical
1188 neuron cultures". 20,000 cells were seeded in white opaque 96 well plates in technical
1189 quadruplicates per embryo per condition. After 7 days *in vitro* neurons were stressed with 250
1190 μM sodium arsenite for 1 hour and recovered respectively. Cell Titer Glo 2.0 Cell Viability
1191 Assay (Promega) was performed on primary cortical neurons following manufacturer
1192 instructions including a standard curve from 0.1 nM to 100 μM ATP in each plate for
1193 standardization. Luminescence was quantified using GLOMAX plate reader and values were
1194 standardized to the luminescence values of the standard curve. The values were then normalized
1195 to the unstressed condition to quantify relative viability during stress and recovery.

1196 ***Behavior testing general information***

1197 All adult behavior testing was performed in the University of Ottawa Behaviour and Physiology
1198 Core. During behavior testing periods the mice were minimally disturbed: food and water were
1199 only added/changed as needed and cages were changed by the experimenter with a transfer of
1200 old bedding material. Apart from nesting and Beam Break testing, all behavior tests were
1201 performed in the light phase of the cycle. The experimenter was blinded to the genotype of the
1202 mice during behavior testing and until the mice were end pointed. Mice were brought to the
1203 testing room to habituate in dim white light at least 30 minutes prior to commencing testing with
1204 the exceptions of nest building and fear conditioning for which there was no habituation period.
1205 The behavior cohort consisted of males and females with 12-15 animals per sex per genotype.
1206 These mice had been backcrossed three times to C57BL/6N background. All mice used for
1207 histology, biochemistry, and RNA analyses performed the fear conditioning test 1 week prior to
1208 dissections to control for potential molecular changes induced by this behavior test.

1209 ***Developmental testing***

1210 A small battery of behavior tests was completed at P8 and P21. At P8, these tested included (I)
1211 weight, (II) righting reflex, (III) hindlimb suspension, and (IV) forelimb suspension. (I) Weight
1212 was measured every other week by placing individual mice on a digital weigh scale. (II) Mice
1213 were placed on their back on a tabletop and timed for how long it took them to right themselves
1214 onto their paws. (III) Mice were placed facing downward in a 50mL Falcon tube (VWR 21008-
1215 940) and timed for their latency to fall. (IV) Mice were placed to grasp a wire suspended by a
1216 pencil holder and timed for latency to fall. At P21, hanging wire was performed in which the
1217 mouse was allowed to grasp a wire 30 cm off the ground and time for its latency to fall. Each
1218 mouse completed three trials with a maximum time of 60 seconds.

1219 ***Beam break***

1220 The Beam Break test was used to assess general locomotor activity and habituation to a novel
1221 cage environment. The apparatuses used to record and analyze the mice activity included the
1222 Micromax analyzer/Fusion Software (Omnitech Electronics; Columbus, OH, USA) at the 2-
1223 month time point and the Photobeam Activity System (San Diego Instruments; San Diego, CA,
1224 USA) at the 9 and 16-month timepoints. Clean cages with only a thin layer of corncob bedding,
1225 food, and water were loaded into the recording frame. Mice were singly housed in one of these
1226 cages 2 hours prior to the start of their dark cycle. For a 24-hour period at the standard 12-hour
1227 dark/light cycle, the activity of the mice was monitored by infrared beam emitters and receptors.
1228 When the test was completed, the sum of the infrared beam breaks in 5-minute, 1-hour, and 24-

hour sampling bins was analyzed.

Digigait

The Digigait treadmill Imager and Analysis Software (Mouse Specifics Inc.) were used to record and analyze parameters of gait, respectively. Mice were placed on the unmoving treadmill surface and once recording was started the speed was increased to 18 cm/s with 0 degree incline. A 3 second video of each mouse walking continuously, with no stopping or starting, was captured. A mouse was excluded from the test if it was unable to walk for 3 seconds at the 18 cm/s speed. Digiait data was analyzed using FactoMinR (*82*) and visualized using FactoExtra (*83*) packages in R (version 4.2.3).

Fear conditioning

Contextual and cued fear conditioning were tested using a 3-day protocol to assess associative fear learning and memory. Naïve age and sex matched mice were initially used to determine the optimal shock value. On day 1 (training), the mice were placed into a Phenotyper box (Noldus Information Technology) with a grid shock floor (Med Associates). The testing room was set to 60 lux light level and 70 dB of white noise (context A). The mice were left in the apparatus for 6 minutes during which they receive 3 tone-shock pairings (30 seconds tone co-terminated with a 2 second foot shock). On day 2 (Context), the mice were placed in the same apparatus (Context A) with no tone or foot shock delivered for the 6-minute trial. On day 3 (cue), the animals were placed in the test apparatus with an altered context (context B) including red light, no white noise, vanilla scent, textured mat covering the shock floor and plastic inserts in the apparatus. The mice are allowed to explore this context with no tone for 3 minutes, and then are presented with the same tone from Day 1 for the last 3 minutes. The time freezing was analyzed with EthoVision software for all 3 testing days.

Grip strength

A grip strength meter (Chatillon DFE II, Columbus Instruments) was used to assess the maximal forelimb grip strength of the mice. The grip strength meter was rotated vertically and temporarily mounted on a flat surface prior to testing. The mouse was brought near the triangular attachment and allowed to grasp the lower bar with its forepaws. The mouse was pulled directly downward, by the tail, in one smooth motion. Each mouse was tested, and the grip strength recorded for 5 consecutive trials with a 1-minute intertrial interval. If a trial was deemed unsuccessful by the blinded experimenter, the trial was redone. Causes of an unsuccessful trial included the mouse prematurely losing its grip on the bar or grasping the bar with its hindfoot. The average grip strength for the 5 successful trials was analyzed.

Hanging wire

The hanging wire test was used to assess muscle strength and coordination. A metal wire was secured to the top of a tall plastic box with padding on the bottom. The mouse was brought near and allowed to grasp the wire with its forepaws. A timer was started once the experimenter released the mouse to allow it to hang freely. When the mouse fell from the wire the time was recorded. Mice had three trials and were allowed to hang for a maximum of 600 seconds with a 60 second intertrial interval in between. If a mouse hung for 600 seconds, it did not complete any additional trials. The maximum hanging time from the trials was used for analysis.

Light/dark box

The light dark paradigm was used to assess anxiety-like or disinhibited, exploratory behavior. The testing apparatus (Med Associates) has two equal sized rectangular compartments the mouse can move freely between. The one is fully illuminated whereas the other is covered by a black plastic insert. The position of the mouse in the apparatus testing field is recorded using infrared beams. To start the test, the mice are placed into the lit side and allowed to explore for 10 minutes. The time spent in each compartment and number of entries into each compartment was recorded and analyzed by Activity Monitor software (Med Associates).

Marble burying

The marble burying assay can assess the motor function required to bury objects as well as cognitive changes related to apathy or perseverance. Cages were filled with 10cm of fresh corncob bedding and one mouse was placed to habituate for 5 minutes. After habituation, 20 glass marbles were laid out evenly in a 4 by 5 pattern. The mouse was returned to the cage and left alone for 30 minutes in 60 lux light. With the completion of the trial, the number of marbles buried by at least two thirds was scored by a blinded experimenter.

Nest building

Nest building is an innate behavior of mice in their daily lives. This complex behavior requires both executive planning and sensorimotor coordination. Directly following Beam Break testing, a single square nestlet (5 cm^2 cotton pad) was placed in each Beam Break cage for 16 – 18 hours, of which 12 of these hours was during the dark cycle. At the end of the test, images were taken of the nests and scored blindly for quality as previously described on a scale from 1-5.

Open field

The open field test was used to assess anxiety and locomotor activity in a novel environment. The apparatus consists of white plastic square arenas measuring 45cm on each side. The mice were placed in a corner of the arena and allowed to freely explore for 10 minutes with light levels at 300 lux. The distance travelled, time spent in the corners and center of the field was recorded and analyzed by EthoVision software (Noldus Information Technology).

Rotarod

The rotarod (IITC Life Science, Ugo Basile) was used to test the motor performance of mice including coordination and resistance to fatigue. Mice were placed in the stationary rotarod bar for 10 seconds before the rotarod program was initiated. The bar accelerated from 4 rpm to 40 rpm for 5 minutes and the latency to fall for each mouse was recorded. The time was stopped when the mouse fell from the bar or rotated passively. Mice were completed four trials per day, with a 10-minute intertrial interval in their home cage, for 3 consecutive days.

Spontaneous Y-maze

The spontaneous Y-Maze test was used to assess spatial working memory. The Y-shaped maze has three identical arms at 120°C around a center point triangle. The mice were placed in the center point and allowed to freely explore the arms for 8 minutes. The movement of the mouse was tracked including the sequence of arm entries by EthoVision (Noldus Information Technology). An alternation is defined as the mouse making consecutive, sequential entries into each of the three arms without revisiting an arm. The alternation index was calculated as (number of alternations/(total number of arm entries minus two)) and reported as a percent.

Tail suspension

1313 The automated Tail Suspension apparatus (Med Associates) was used to assess apathetic-like
1314 behaviors of the mice. Mice were taped and suspended by the tail to a vertical steel bar which
1315 measures strain gauge as the mouse moves during a 6-minute trial. The cumulative time spent
1316 immobile, hanging passively (below lower threshold) was measured by the Tail Suspension
1317 software.

1318 ***Three chamber sociability***

1319 The Three Chamber test was conducted to measure the sociability of mice when allowed to
1320 interact with a novel mouse or a similarly sized inanimate object. The testing apparatus is a 19 x
1321 45 cm plastic box divided into three equal chambers with clear plastic wall dividers. The two
1322 external chambers each have a single weighted metallic mesh pencil holder and the central
1323 chamber is empty. The mice are habituated to the apparatus for 5 minutes by being placed in the
1324 central chamber and allowed to freely explore and enter all chambers. The mouse has a 5-minute
1325 intertrial interval in its home cage. In the test trial, a sex and age matched wild-type mouse
1326 (social target) is placed beneath one mesh pencil holder, and an inanimate plastic toy (non-social
1327 target) is placed beneath the other. To commence the test trial, the mouse is paced in the central
1328 chamber. The time spent in each chamber and interacting with the social or non-social target is
1329 recorded and analyzed by EthoVision software (Noldus Information Technology).

1330 ***Tube test of social dominance***

1331 Tube test was used to assess social dominance and within cage social hierarchy. Cage mates
1332 were paired against each other for testing in a round-robin design. The tube test was conducted
1333 on a flat tabletop, which the mice were allowed to run around on for 5 minutes prior to
1334 commencing the testing. One foot of vinyl tubing was used. Mice were habituated to the tube
1335 prior to testing on the same day by encouraging them to run through the empty tube from either
1336 side 5 times. A blinded experimenter placed a mouse on either end of the tube, and released their
1337 tales when they completely entered the tube. The first mouse to step its hind paws out of the tube
1338 lost the battle. The battle was redone if after 2 minutes no mouse had won.

1339 ***Collection and preparation of mouse tissue***
1340 Mice were harvested for both histology and biochemistry/molecular analyses to reduce total
1341 animal numbers. Mice were first acclimated for 2 hours prior to dissection to help control for
1342 activity-induced changes and all dissections were performed at zeitgeber hours ZT6 to ZT11 to
1343 control for potential circadian affects. Mice were randomly dissected by cage to limit batch
1344 effects and additional stress. Mice were anesthetized using isoflurane inhalation, blood was
1345 collected, and then mice were sacrificed via decapitation and the brains were quickly isolated,
1346 weighted, then cut into 2 hemispheres where the left hemisphere was drop fixed in 10% buffered
1347 formalin and the right hemisphere was dissected by region and flash frozen on dry ice. Spinal
1348 cords were removed using hydraulic extrusion and the lumbar spinal cord was isolated. The
1349 lumbar enlargement was isolated for histology whereas the remaining lumbar spinal cord was
1350 used for molecular analysis. Tibialis anterior and soleus muscles were isolated and drop fixed in
1351 10% buffered formalin for imaging studies and gastrocnemius muscle was flash frozen.

1352 ***Immunofluorescence analysis in mouse tissue***

1353 Tissue was collected as described in *Collection and preparation of mouse tissue*. Following
1354 fixation for 48 hours, spinal cord samples were transferred to a 70% ethanol solution and sent to
1355 the Louise Pelletier Histology Core facility at the University of Ottawa for paraffin embedding

1356 and microtome sectioning. The samples were sectioned at a thickness of 5 µm. Serial sectioning
1357 was performed at four levels within the tissue each separated by 40 µm. For staining, slide-
1358 mounted sections were deparaffinized in 100% xylenes (Fisher Scientific X3P-1GAL) for 10
1359 minutes, then transferred into a second container of fresh 100% xylenes for an additional 10
1360 minutes. The slides were then rehydrated in descending ethanol solutions: two 5 minutes
1361 treatments in 100% ethanol, 5 minutes in 70% ethanol, and 5 minutes in 50% ethanol. The slides
1362 were then immersed in 1X PBS for at least 5 minutes to rinse residual ethanol. Antigen was
1363 performed by placing slides in 1X sodium citrate buffer (2.94g sodium citrate 0.5mL Tween-20
1364 in 1L 1X PBS, pH6) at 95°C for 30 minutes then rinsed in 1X PBS. Tissue sections were then
1365 blocked in blocking buffer containing 1% Triton-X and serum (5% horse serum, 5% cosmic calf
1366 serum, or 1% bovine serum albumin) in 1X PBS for 2 hours at room temperature. Next the tissue
1367 sections were incubated with primary antibody (table S5) overnight at 4°C. The next day, the
1368 sections were washed twice in PBS 1X + 0.1% Triton-X for 5 minutes each and then 3X in 1X
1369 PBS for 5 minutes each. The slides were then incubated in secondary antibody at room
1370 temperature for 2 hours. The slides were then washed in 1X PBS + 0.1% Triton-X for 5 x 5-
1371 minutes, before mountin with #1.5 coverslips (Thermo Fisher Scientific 12-544E) and
1372 fluorescent mounting media (Dako S3023). The coverslips were sealed with clear nail polish and
1373 allowed to dry before imaging. Images of each ventral horn were taken on a Zeiss Axio Imager 2
1374 at 20X magnification. Cells were counted manually per image using Fiji (ImageJ).

1375 ***Neuromuscular junction analysis***

1376 Tissue was collected as described in *Collection and preparation of mouse tissue*. After 24 hours
1377 of fixation, tibialis anterior muscles were stored in a solution of 1X PBS. Muscle bundles were
1378 carefully teased apart from the tissue into 4-5 bundles with forceps. The muscle bundles were
1379 transferred to 6-well plate cell culture plate containing 1% Triton-X in 1X PBS overnight at 4°C
1380 under gentile agitation for permeabilization. The next day, the muscle bundles were washed three
1381 times in 1X PBS for 5 minutes at room temperature. They were placed in a blocking buffer
1382 solution of 4% bovine serum albumin and 1% Triton-X in 1X PBS at 4°C overnight. The
1383 following day, the muscles were incubated in primary antibody (BTX and NfL/SV2 cocktail, see
1384 table S5) diluted in blocking buffer solution overnight at 4°C. The next day, the muscle bundles
1385 were washed with 1X PBS three times for 5 minutes and incubated with secondary antibody
1386 diluted in blocking buffer solution at room temperature for 2 hours. The muscle bundles were
1387 then washed 3 times in 1X PBS for 5 minutes. The bundles were then placed on slides, mounted
1388 with VECTASHIELD® HardSet™ Antifade Mounting Medium (#H-1400), and #1.5 coverslips
1389 placed above the muscle bundles. The slides were left at room temperature overnight in the dark
1390 to allow the mounting media to cure. Images were taken on a Zeiss LSM800 Confocal
1391 Microscope at 20X through a Z-stack with optimal spacing (0.61 µm). Images were taken
1392 throughout the entirety of the muscle tissue such that at least 80 neuromuscular junctions per
1393 animal were captures. Images were scored manually per image using Fiji (ImageJ). See fig.
1394 S10C for scoring examples.

1395 ***SUMOylation analysis in human brain tissue***

1396 20 mg of frozen human brain tissue was homogenized in 300 µL of RIPA buffer supplemented
1397 with protease inhibitor, phosphatase inhibitor, and 50mM N-Ethylmalamide and vortexed every
1398 5 minutes for 20 minutes while incubating on ice. The samples were centrifuged at 21000G for
1399 20 minutes at 4°C and the supernatant (RIPA soluble fraction) was carefully removed. 4X
1400 laemmli buffer was added and samples were boiled for 5 minutes at 95 °C then stored overnight

1401 at 4 °C. The remaining pellet after the centrifugation step post-lysis was washed in 1mL RIPA
1402 buffer with vortexing for 10 seconds followed by centrifugation at ~21000G for 20 minutes at 4
1403 °C. The supernatant was carefully removed, and the pellet was resuspended in 300 µL of of 8M
1404 UREA in PBS with 10mM Tris-HCl pH 7.4. Samples were vortexed and left to solubilize
1405 overnight at room temperature before 4X Laemmli was added prior to Western Blot analysis.
1406 RIPA and UREA samples were randomly loaded onto gels (separated by fraction) with 4 control
1407 samples consistently loaded (aged 20-30) on each gel for normalization. Western blot was
1408 performed as described above. Samples were standardized to ponceau signal then normalized to
1409 control samples.

1410 ***Collection and preparation of FFPE human brain tissue***

1411 Frontal cortex tissues were collected antemortem from three sporadic ALS/FTLD patients (a 74-
1412 year-old male, 67-year-old female and 59-year-old female) obtained through the ALS Clinic at
1413 Sunnybrook Health Sciences Centre, Toronto. ALS was diagnosed using the revised El Escorial
1414 Criteria (Brooks et al., 2000) and informed consent was obtained with approval from the local
1415 ethical review board. The presence of TDP-43 proteinopathy within the frontal cortex was
1416 verified through immunohistochemical labeling using rat anti-phosphorylated TDP-43
1417 (p409/410) antibody on formalin fixed paraffin embedded sections. Genetic analyses confirmed
1418 absence of mutations in key ALS/FTD-associated genes: *C9orf72*, *SOD1*, *FUS* and *TARDBP*.

1419 ***Proximity ligation assay in human FFPE tissue***

1420 Formalin fixed paraffin-embedded human brain sections (5 µm sections) were deparaffinized
1421 using two 10-minute washes with xylenes, two 5-minute washes with 100% ethanol, one 5-
1422 minute wash with 70% ethanol, and one 5-minute was with 50% ethanol. Deparaffinized sections
1423 then underwent sodium citrate antigen retrieval (10mM sodium citrate, 0.05% Tween-20, pH 6)
1424 for 2 hours at 80°C. Sections were then blocked with Duolink blocking buffer (Sigma Aldrich,
1425 DUO82007) for 1 hour at room temperature. Next, sections were incubated with primary
1426 antibodies (anti-TDP-43 1:750, PTGLabs; anti-SUMO2/3 [8A2] 1:500 Sigma) diluted in
1427 blocking buffer (1.5% Triton X-100, 10% cosmic calf serum in 1X PBS) overnight at 4°C. The
1428 following day, the sections were washed in Duolink Wash Buffer A (0.01M Tris-Base, 0.15M
1429 NaCl, 0.05% Tween-20, pH 7.4), followed by incubation in Duolink PLA MINUS (Sigma
1430 Aldrich, DUO82004) and PLUS probes (Sigma Aldrich, DUO82002) at 37°C for 1 hour.
1431 Duolink PLA probes were diluted in antibody diluent (Sigma Aldrich, DUO82008) at a 1:5
1432 dilution. Sections were washed in Duolink Wash Buffer A and then incubated in ligase (Sigma
1433 Aldrich, DUO82027) at 37°C for 30 minutes. Ligase was diluted in 1X ligation buffer (Sigma
1434 Aldrich, DUO82009) at a 1:40 dilution. Then, the sections were washed in Duolink Wash Buffer
1435 A and then incubated in polymerase (Sigma Aldrich, DUO82028) at 37°C for 90 minutes.
1436 Polymerase was diluted in 1X amplification buffer (Sigma Aldrich, DUO82011) at a 1:80
1437 solution. The sections were then washed in Duolink Wash Buffer B (0.2M Tris-Base, 0.1M
1438 NaCl, pH 7.5) and then again in Duolink Wash Buffer B diluted at 1:1000. Finally, sections were
1439 incubated with DAPI at room temperature for 15 minutes. DAPI was diluted at 1:1000 in PBS.
1440 Fluorescent mounting media (Dako, S3023) and #1.5 coverslips were then placed over the
1441 sections and sealed using clear nail polish. Images were taken on a Zeiss LSM800 Confocal
1442 Microscope. 5 images per tissue were randomly collected from grey matter at 63X magnification
1443 and 2X digital zoom through a Z stack of 10-12 µm with optimal spacing (0.27 µm) at a
1444 resolution of 512 x 512 pixels. PLA foci were manually counted per image using Fiji (ImageJ).

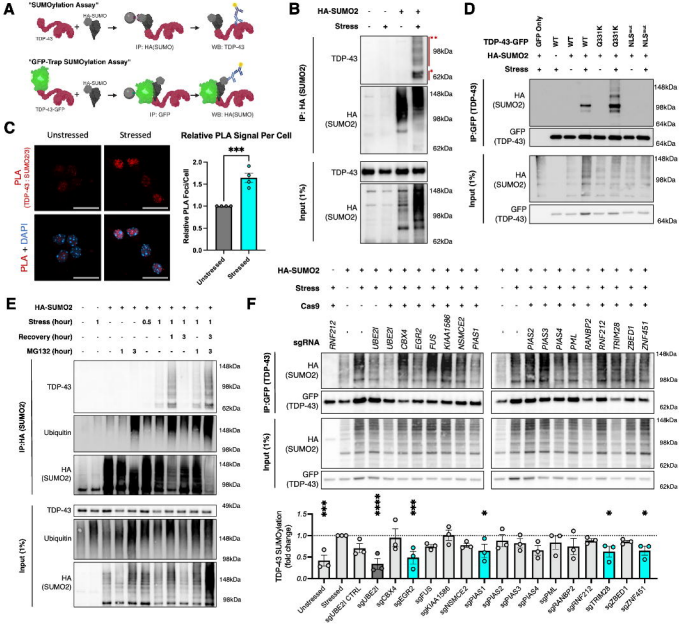

Fig. 1: SUMOylation dynamically regulates nuclear TDP-43 in a stress-responsive manner.

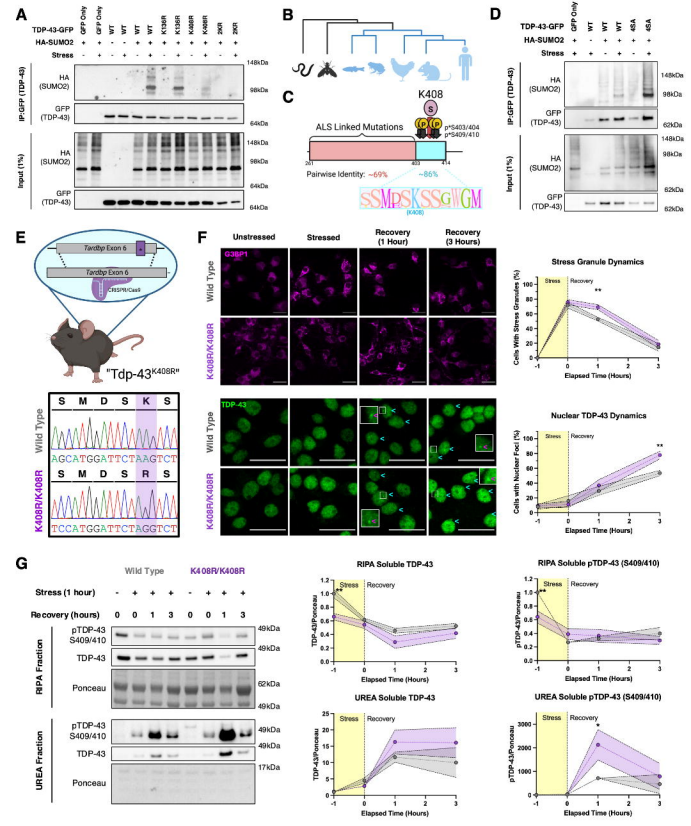

Fig. 2: Blocking TDP-43 SUMOylation at conserved K408 impairs the cellular stress response.

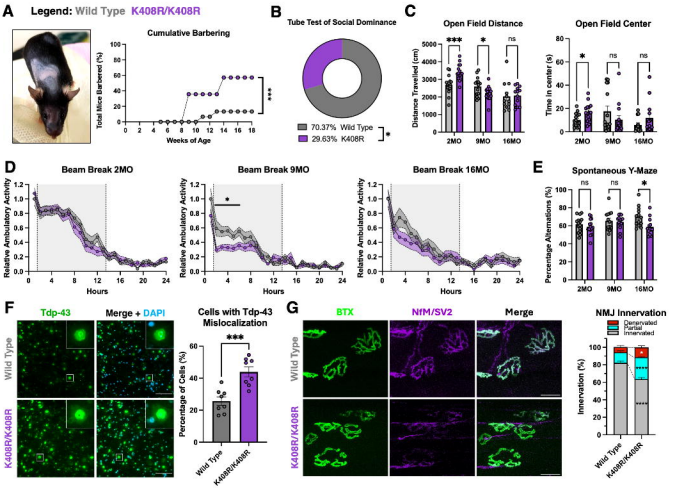

Fig. 3: Blocking TDP-43 SUMOylation *in vivo* leads to sex-specific and age-dependent impairment and pathology.

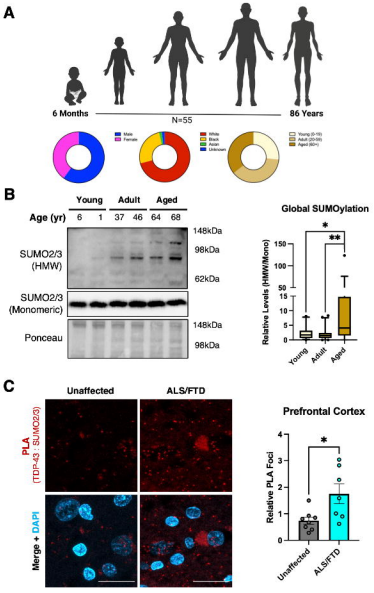

Fig. 4: SUMOylation correlates with aging and is enriched in the prefrontal cortex of ALS/FTD patients.